Sensitivity of Lag-Damping Correlations to Structural and Aerodynamic Approximations of Isolated Experimental Rotors in Forward Flight

INTERIM
IN-02-CR
IREF.
8441
44P

Interim Technical Report Under NASA-Ames Research Grant No. NAG 2-797
(August 1, 1992 - December 21, 1993)

G. H. Gaonkar
S. Subramanian
Srinivas Chunduru

Prepared for the Aeroflightdynamics Directorate
U. S. Army Aviation Research and Technology Activity
Ames Research Center
Moffett Field, CA 94035

FLORIDA ATLANTIC UNIVERSITY
Department of Mechanical Engineering
College of Engineering
Boca Raton, FL 33431

April 1994

CASI

Scope of NASA-Ames Research Grant No. NAG 2-797, 1 August 1992 - 31 July 1994.

Work under this agreement started on August 1, 1992. The papers resulting from this study are

1) Barwey, D. and Gaonkar, G. H., "Effects of Dynamic Stall and Structural Modeling on Helicopter Blade Stability with Experimental Correlation," *AIAA Journal*, Vol. 32, (5), May 1994 (in press).

2) Manjunath, A. R., Nagabhushanam, J., Gaonkar, G. H., Srinivas Chunduru and Prasad Sampath, "Flap-Lag-Torsion Stability in Hover and Forward Flight With a Three-Dimensional Wake," Proceedings of the American Helicopter Society Aeromechanics Specialists Conference, San Francisco, CA, Jan 18-21, 1994.

3) Gaonkar, G. H., Nakadi, R. M., Subramanian, S. and Nagabhushanam, J., "Parallel-Computing Concepts and Methods Toward Large-Scale Floquet Analysis of Helicopter Trim and Stability," Proceedings of the American Helicopter Society Aeromechanics Specialists Conference, San Francisco, CA, Jan 18-21, 1994.

4) Subramanian, S., Srinivas Chunduru and Gaonkar, G. H., "Effects of Dynamic Stall and Three-Dimensional Wake on Aeroelastic Stability of Isolated Hingeless Rotors with Experimental Correlation," accepted for presentation at the American Helicopter Society 50th Annual Forum, Washington, DC, May 11-13, 1994.

5) Achar, N. S. and Gaonkar, G. H., "An Exploratory Study of a Subspace Iteration Method as an Alternative to the QR Method for Floquet Eigenanalysis," *Journal of Mathematical and Computer Modeling* (in press).

Summary

The predictions of regressive lag-mode damping levels are correlated with the database of an isolated, soft-inplane, three-blade rotor operated untrimmed. The database was generated at the Army Aeroflightdynamics Directorate at Ames. The correlation covers a broad range of data, from near-zero thrust conditions in hover to high-thrust and highly stalled conditions in forward flight with advance ratio as high as 0.55 and shaft angle as high as 20^0. In the experimental rotor, the airfoil or blade portion has essentially uniform mass and stiffness distributions, but the root flexure has highly nonuniform mass and stiffness distributions. Accordingly, the structural approximations refer to four models of root-flexure-blade assembly. They range from a rigid flap-lag model to three elastic flap-lag-torsion models, which differ in modeling the root flexure. The three models of root-flexure are: 1) three root springs in which the bending-torsion couplings are fully accounted for; 2) a finite-length beam element with some average mass and stiffness distributions such that the fundamental frequencies match those of the experimental model; and 3) accurate modal representation in which the actual mass and stiffness distributions of the experimental root-flexure-blade assembly are used in calculating the nonrotating mode shapes. The four models of root-flexure-blade assembly are referred to as the rigid flap-lag model, spring model, modified model and modal model. For each of these four models of the root-flexure-blade assembly, the predictions are based on the following five aerodynamic theories: (i) *linear theory*, which accounts for large angle-of-attack and reverse-flow effects on lift, and has constant drag and pitching moment; (ii) *quasisteady stall theory*, which includes quasisteady stall lift, drag and pitching moment characteristics of the airfoil section; (iii) *dynamic stall theory*, which uses the ONERA dynamic stall models of lift, drag and pitching moment; (iv) *dynamic wake theory*, which is based on a finite-state three-dimensional wake model and includes all wake effects including both shed and trailing vorticity; and (v) *dynamic stall and wake theory*, which combines both dynamic stall theory and dynamic wake theory and is a relatively complete aerodynamic representation. The number of modes in the modal representation, the number of radial shape functions and temporal harmonics in the wake representation and the number of blade elements in the dynamic stall representation are gradually increased for converged results of damping. The periodic forced response and the Floquet transition matrix about that response are obtained by

periodic shooting; the damping levels are generated from a full Floquet eigenanalysis that includes all the structural and aerodynamic states. The correlation demonstrates the need to include dynamic stall and three-dimensional wake in lag-damping predictions.

Notation

Unless otherwise stated, the symbols below are dimensionless:

a	linear lift curve slope, (rad^{-1})
a_d, a_m	damping factors in dynamic stall drag and pitching moment models
b	airfoil semi-chord, (1/R)
c	airfoil chord, (1/R)
C_d, C_{d_0}	airfoil sectional drag coefficient and constant profile drag coefficient
C_l, C_m	airfoil lift and pitching moment coefficients
C_{m_0}	airfoil pitching moment coefficient at zero angle of attack
C_T	thrust coefficient
e	phase shift parameter for dynamic stall lift
e_h	blade hinge offset for the spring model (Fig. 2a), (1/R)
e_l	length of the hub segment in modified model (Fig. 2b), (1/R)
E_d, E_m	phase shift parameters in dynamic stall drag and pitching moment models
j	polynomial number
k	b/x
K_β, K_ζ	root spring rates in flap and lag, respectively (Fig. 2a), (Nm/rad)
K_ϕ	root spring rate in torsion (Fig. 2a), (Nm/rad)
l	length of the blade from the hinge to tip (equal to $1-e_h$ for the spring model and $1-e_l$ for the modified model)
L_i	blade sectional lift of the i-th blade, (N/m)
L_x, L_y	local aerodynamic forces (Fig. 3), ($1/\rho b\Omega^2R^3$)
L_0	apparent mass lift normal to the chord line, ($1/\rho b\Omega^2R^3$)

$[L_c]$, $[L_s]$	influence coefficient matrices
m	harmonic number
M	aerodynamic pitching moment, $(1/\rho b\Omega^2R^4c)$
M_0	noncirculatory aerodynamic pitching moment per unit length, $(1/\rho b\Omega^2R^4c)$
[M]	mass matrix
n	polynomial number
$\bar{P}_n^m(\bar{r}_i)$	normalized Lengendre Polynomial (n,m) of the first kind
Q	number of blades
r	harmonic number
r_d, r_m	frequency parameters in dynamic stall drag and pitching moment models
r_f	length of the root flexure (Fig. 2b), (1/R)
$\bar{r}_i$	radial station of the i-th blade, (1/R)
R	rotor radius, (m)
$\mathcal{R}$	flap-lag structural coupling ratio
t	time parameter
u	axial deflection, (1/R)
U	resultant air velocity at a blade station (Fig. 3), $(1/\Omega R)$
v	lag bending deflection, (1/R)
V	inflow parameter
V_t	total inflow parameter
[V]	diagonal matrix with elements V_t, V, V, ···, V
w, d	dynamic stall lift frequency and damping parameters
w	flap bending deflection, (1/R)
x	radial distance measured from the rotor center, (1/R)
α	blade airfoil section angle of attack, (rad)
α_j^r, β_j^r	wake states
α_s	shaft-tilt angle, (deg)

Γ	circulation per unit length, UC_l
Γ_d	circulation-like drag per unit length, UC_d
Γ_m	circulation-like pitching moment per unit length, UC_m
δ	pitch-rate coefficient, (rad^{-1})
δ_m	pitching-moment parameter
$\dot{\varepsilon}$	airfoil rotation rate with respect to airmass
θ_f	pre-pitch of the root-flexure (Fig. 2a), (deg)
θ_0	collective pitch angle, (deg)
λ	time-delay parameter
λ_t	total inflow
$\lambda(\bar{r}_i, \psi_i, t)$	downwash on the i-th blade
λ_m	thrust induced inflow
μ	advance ratio
ϕ	elastic twist, (rad)
$\phi_j^r(\bar{r}_i)$	radial shape functions
	$\phi_j^r(\bar{r}_i) = \frac{1}{\nu}\bar{P}_j^r(\nu);\ \nu = \sqrt{(1-\bar{r}_i^2)}$
ϕ_0	elastic twist at the blade root in Fig. 2a, (rad)
σ	negative of lead-lag mode damping exponent, (1/sec)
σ_s	rotor solidity
ψ_i	azimuthal location of the i-th blade
ρ	air density (kg/m^3)
Ω	rotor angular speed, (rad/sec)
τ_n^{mc}, τ_n^{ms}	inflow forcing functions
$(\,)_1$, $(\,)_2$	unstalled and stalled components
$(\,)_x$, $(\,)_y$	x and y components
$(\dot{x})$	time derivative of x

$\approx$ approximately equal to

Introduction

The current capability to predict helicopter lag damping needs significant improvements. Four considerations make the prediction difficult and motivate the present investigation based on Floquet theory. First, drag, induced drag and Coriolis forces are delicately balanced in the inplane direction. Therefore, from hovering to high-speed flights, a wake representation that goes well beyond dynamic-inflow and lift-deficiency-type approximations is required (Ref. 1). Second, with increasing demand on the stability margins of high-speed and highly maneuverable helicopters, high-thrust conditions in forward flight become increasingly important. Thus, the complex phenomenon of dynamic stall becomes an issue (Refs. 2-4) and needs to be accounted for as well. Third, lag-damping prediction is sensitive to modeling the rotor system and its flow field. It is also sensitive to the accuracy of computing the periodic forced response, the Floquet transition matrix about that response and the eigenvalues of this matrix. Thus, it is important that a consistent sophistication is maintained from modeling to response analysis to eigenanalysis. Often this requires that all the structural and aerodynamic states are included not only in response analysis but also in eigenanalysis (Ref. 5). This is a demanding and expensive exercise; with lag bending, flap bending and torsional degrees of freedom, even simplified research models of multiblade rotors with wake and stall dynamics routinely lead to nearly 200 structural and aerodynamic states for converged results. Fourth, given the complexity of the rotor system and its flow field, it becomes necessary that the predictions are checked against a broad range of model test data. Currently the database is severely limited. Although not typical of operational rotor systems, the database due to McNulty is an exception (Ref. 6). It is comprehensive to include near-zero thrust conditions in hover and forward flight to high-thrust and highly stalled conditions in forward flight ($0 \le \mu \le 0.55$, $0^0 \le \theta_0 \le 6^0$, $0^0 \le \alpha_s \le 20^0$); for details, see Refs. 2 and 7.

Given this background, we review the aeroelastic stability studies with dynamic stall and/or three-dimensional wake modeling. The use of both stall and three-dimensional wake modeling is almost routine

in loads and vibration studies. By comparison their use is far less common in stability studies. Perhaps the first study to consider their use is due to Torok and Chopra (Ref. 4), who also provide a review of aeroelastic stability modeling through 1991. However, in Ref. 4, stall and free wake are included in trim analysis, but they are frozen in dynamic perturbation. Thus, the important effects of wake and stall on trim analysis are included, but their effects on eigenanalysis are not. Moreover, Ref. 4 uses only a lightly loaded section of the database of Ref. 6 (shaft tilt $\alpha_s \leq 10^0$ and collective pitch $\theta_0 \leq 3^0$). Thus, an appreciable section of the database under high shaft-angle and collective-pitch conditions ($\alpha_s \leq 20^0$ and $\theta_0 \leq 6^0$) is not included. Developments since 1991 include the works of Barwey et al. (Refs. 2 and 3), who use dynamic stall modeling and provide correlation with virtually the complete database of Ref. 6. While a rigid flap-lag model is used in Ref. 2, two elastic flap-lag-torsion models that differ in simulating the root flexure are used in Ref. 3. Manjunath et al. (Ref. 1) use a finite-state three-dimensional wake model and rigid flap-lag modeling. Reference 1 also includes limited correlation with test data of Ref. 6 under low-thrust conditions. The work in Ref. 1 is extended in Ref. 8 to include elastic blade modeling. References 1 and 8 also include a review of aeroelastic stability predictions with the use of dynamic wake modeling.

In this study, we investigate the sensitivity of lag-damping correlations to structural and aerodynamic approximations of isolated, hingeless experimental rotors in forward flight. Virtually the complete database of Ref. 6 is used. We use the ONERA dynamic stall models of lift, drag and pitching moment. The unsteady wake is described by a finite-state three-dimensional wake model. The blade dynamics is represented by a rigid blade model as well as by three elastic blade models, which differ in modeling the root flexure (details to follow). In order to isolate different aerodynamic aspects of the stability problem, predictions based on the linear (quasisteady) and quasisteady stall theories are included as well. Highly stalled cases would merit further research; nevertheless, their inclusion provides additional opportunities to examine how far we can use Floquet theory and the very concept of modal damping (Ref. 9). Thus, in summary, the predictions are based on a broad range of structural and

aerodynamic representations, and they are correlated with a comprehensive database (Ref. 6). Such a correlation should provide a useful reference.

Modeling

The correlation study requires an adequate model of the root-flexure-blade assembly of the three-blade experimental rotor (see Fig. 1), which was designed to represent a simple model of a hingeless rotor with spring restrained flap-lag hinges. While the mass and stiffness distributions are essentially uniform for the blade portion, they are highly nonuniform for the root flexure or root beam. According to Ref. 3, the sensitivity of lag-damping predictions to the structural refinements in modeling the root-flexure-blade assembly increases with increasing blade pitch and advance ratio. Therefore, to bracket the extent of this sensitivity to modeling details, we use four models of the root-flexure-blade assembly. They range from a rigid flap-lag blade model to three elastic flap-lag-torsion models, which have identical blade representation but differ in root-flexure representations. All the models have the capacity to simulate full and zero structural flap-lag couplings ($\mathcal{R}$ = 1 and $\mathcal{R}$ = 0) of the experimental model. The lag-damping predictions are based on five aerodynamic theories, which range from linear (quasisteady) theory to a relatively comprehensive dynamic stall and wake theory. To simplify the subsequent presentation of results and clarify terminology, we briefly describe these four models of root-flexure-blade assembly and the five aerodynamic theories.

Root-Flexure-Blade Assembly

Rigid Flap-Lag: It is an offset-hinged rigid blade with flap and lag (inplane) degrees of freedom; the flap and lag hinges are spring restrained and coincident (Ref. 2).

Spring Model: The root-flexure is simulated by a set of three linear springs located at an effective hinge offset as shown in Fig. 2a; the spring stiffnesses are based on measured values. The airfoil or the blade portion has uniform mass and stiffness distributions. The bending-torsion couplings of the root spring system are fully accounted for (Ref. 3).

Modified Model: The root flexure is simulated by a short beam, over which the mass and stiffness properties are kept uniform; see Fig. 2b. Their magnitudes are chosen so as to reasonably match the fundamental, nonrotating bending and torsion frequencies of the experimental model, and thus to those of the spring model. With judicious choice of hinge offset and the length of root beam it is possible to match the nonrotating and rotating frequencies of the first two flap-bending, lag-bending and torsional modes of the spring model (Ref. 3).

Modal Model: The actual mass and stiffness distributions of the root-flexure-blade assembly of the test model are used in calculating the nonrotating mode shapes numerically. For illustration, the flap and lag stiffness distributions are sketched in Fig. 2c for the three-blade experimental rotor (Ref. 6); the torsional stiffness, omitted for clarity of graphical representation, is equally nonuniform with steep gradients.

Aerodynamics

The aerodynamic representation called the dynamic stall and wake theory is fairly comprehensive. It includes the effects of dynamic stall lift, drag and pitching moment from a thin airfoil theory (Refs. 10 and 11) and the downwash effects from a finite-state three-dimensional wake theory (Ref. 12). Moreover, the airfoil theory includes the effects of reversed flow and large angles of attack, and the wake theory accounts for the finite number of blades. We begin with a brief account of dynamic stall theory. This is followed by a discussion of how quasisteady stall and linear theories are derived as special cases. After introducing dynamic wake theory, we conclude this section with a mention of dynamic stall and wake theory.

Dynamic Stall Theory: It is based on the ONERA models of unified lift, drag and pitching moment. Basically we introduce lift circulation Γ, circulation-like drag Γ_d and circulation-like pitching moment Γ_m as follows:

$$\Gamma = \Gamma_1 + \Gamma_2,\ \Gamma_d = \Gamma_{d1} + \Gamma_{d2},\ \Gamma_m = \Gamma_{m1} + \Gamma_{m2} \tag{1}$$

where subscripts 1 and 2 indicate the linear and stalled or nonlinear components, respectively. These six components, two each in lift, drag and pitching moment, are governed by Eqs. (2) - (4).

Dynamic Stall Lift:

$$k\dot{\Gamma}_1 + \lambda\Gamma_1 = \lambda a(U_y + b\dot{\varepsilon})\cos\alpha + \delta b\dot{\varepsilon} \tag{2a}$$

$$k^2\ddot{\Gamma}_2 + 2dwk\dot{\Gamma}_2 + w^2(1+d^2)\Gamma_2 = -w^2(1+d^2)\left[U\Delta C_z + ek(\dot{U}_x\cos\alpha + \dot{U}_y\sin\alpha)\Delta C_z + ek(\dot{U}_y\cos\alpha - \dot{U}_x\sin\alpha)\frac{\partial\Delta C_z}{\partial\alpha}\right] \tag{2b}$$

Dynamic Stall Drag:

$$\Gamma_{d_1} = UC_{d_0} \tag{3a}$$

$$k^2\ddot{\Gamma}_{d_2} + a_d k\dot{\Gamma}_{d_2} + r_d^2\Gamma_{d_2} = -\left[r_d^2 U\Delta C_d + E_d k\dot{U}_y\right] \tag{3b}$$

Dynamic Stall Pitching Moment:

$$\Gamma_{m_1} = UC_{m_0} + \delta_m b\dot{\varepsilon} \tag{4a}$$

$$k^2\ddot{\Gamma}_{m_2} + a_m k\dot{\Gamma}_{m_2} + r_m^2\Gamma_{m_2} = -\left[r_m^2 U\Delta C_m + E_m k\dot{U}_y\right] \tag{4b}$$

Thus, it is seen that the linear components in Eqs. (2a), (3a) and (4a) follow the classical thin-airfoil theory. By comparison, the stalled components have an involved algebraic structure and merit additional comments. For example, in Eqs. (2b), (3b) and (4b), ΔC_z, ΔC_d and ΔC_m act like driving forces and represent the differences between the linear and quasisteady values of the airfoil section characteristics. For example, ΔC_z at an instantaneous angle of attack α is the difference between the extrapolated linear lift coefficient and the quasisteady stall lift coefficient of the airfoil; for details, see Ref. 13. Similarly, λ, δ, d and w in the lift equation, a_d, r_d and E_d in the drag equation and δ_m, a_m, r_m and E_m in the pitching-moment equation are determined on the basis of wind-tunnel experiments. Another important parameter in the linear part of the lift equation is $\dot{\varepsilon}$, which represents the airfoil rotation rate relative to airmass and includes complete geometric rotations of the airfoil.

It is expedient to represent the above airfoil lift Γ, drag Γ_d and pitching moment Γ_m in the local airfoil coordinates in terms of L_x, L_y and M as shown in Fig. 3. This is done in Eqs. (5a)-(5c).

$$L_y = U_x\left[\Gamma_1 + \Gamma_2\right] + U_y\left[\Gamma_{d1} + \Gamma_{d2}\right] + L_0 \tag{5a}$$

$$L_x = -U_y\left[\Gamma_1 + \Gamma_2\right] + U_x\left[\Gamma_{d1} + \Gamma_{d2}\right] \tag{5b}$$

$$M = 2b\left[U(\Gamma_{m1} + \Gamma_{m2})\right] + M_0 \tag{5c}$$

where L_0 and M_0 are apparent mass lift normal to the chord and noncirculatory pitching moment at the three-quarter chord point.

Quasisteady Stall Theory: It includes the airfoil-section quasisteady stall characteristics. From Eqs. (2)-(4), by suppressing dynamic stall characteristics we get

$$\Gamma_1 = a(U_y + b\dot{\varepsilon})\cos\alpha; \quad \Gamma_2 = -U\Delta C_z \tag{6a}$$

$$\Gamma_{d_1} = UC_{d_0}; \quad \Gamma_{d_2} = -U\Delta C_d \tag{6b}$$

$$\Gamma_{m_1} = UC_{m_0} + \delta_m b\dot{\varepsilon}; \quad \Gamma_{m_2} = -U\Delta C_m \tag{6c}$$

Linear Theory: Similarly, by suppressing the quasisteady stall characteristics, the equations of lift, drag and pitching moment, including effects of reversed flow and large angles of attack, are:

$$\Gamma_1 = a(U_y + b\dot{\varepsilon})\cos\alpha; \quad \Gamma_2 = 0 \tag{7a}$$

$$\Gamma_{d_1} = UC_{d_0}; \quad \Gamma_{d_2} = 0 \tag{7b}$$

$$\Gamma_{m_1} = UC_{m_0} + \delta_m b\dot{\varepsilon}; \quad \Gamma_{m_2} = 0 \tag{7c}$$

Dynamic Wake Theory: It is linear theory with downwash dynamics, which is modeled by a finite-state three-dimensional wake theory due to Peters, Boyd and He (Ref. 12). At a blade station with radial coordinate $\bar{r}_i$ and spatial azimuth ψ_i, the instantaneous wake or downwash $\lambda(\bar{r}_i, \psi_i, t)$ is given by a complete set of radial shape functions $\phi_j^r(\bar{r}_i)$ and spatial harmonics $\cos(r\psi_i)$ and $\sin(r\psi_i)$:

$$\lambda(\bar{r}_i, \psi_i, t) = \sum_{r=0}^{\infty} \sum_{j=r+1, r+3}^{\infty} \phi_j^r(\bar{r}_i)\left[\alpha_j^r(t)\cos(r\psi_i) + \beta_j^r(t)\sin(r\psi_i)\right] \tag{8}$$

The cosine component $\alpha_j^r(t)$ and the sine component $\beta_j^r(t)$ are the dynamic states of the downwash and are governed by

$$[M]\left\{\dot{\alpha}_j^r\right\} + [V][L_c]^{-1}\left\{\alpha_j^r\right\} = 0.5\left\{\tau_n^{mc}\right\}$$

$$[M]\left\{\dot{\beta}_j^r\right\} + [V][L_s]^{-1}\left\{\beta_j^r\right\} = 0.5\left\{\tau_n^{ms}\right\} \tag{9}$$

where $[V]$ is the diagonal matrix with $V_{11} = V_t = \sqrt{(\mu^2 + \lambda_t^2)}$ and all other elements are given by $V = (\mu^2 + (\lambda_t + \lambda_m)\lambda_t) / \sqrt{(\mu^2 + \lambda_t^2)}$. Closed-form expressions are available for the diagonal mass matrix [M] and influence coefficient matrices $[L_c]$ and $[L_s]$. Similarly, τ_n^{mc} and τ_n^{ms} are cosine and sine components of the pressure coefficient, which, for a rotor with Q blades, are given by

$$\tau_n^{0c} = \frac{1}{2\pi} \sum_{i=1}^{Q} \int_0^1 \frac{L_i \phi_n^0(\bar{r}_i)}{\rho \Omega^2 R^3} d\bar{r}_i$$

$$\tau_n^{mc} = \frac{1}{\pi} \sum_{i=1}^{Q} \int_0^1 \frac{L_i \phi_n^m(\bar{r}_i)}{\rho \Omega^2 R^3} d\bar{r}_i \cos(m\psi_i)$$

$$\tau_n^{ms} = \frac{1}{\pi} \sum_{i=1}^{Q} \int_0^1 \frac{L_i \phi_n^m(\bar{r}_i)}{\rho \Omega^2 R^3} d\bar{r}_i \sin(m\psi_i) \qquad (10)$$

Dynamic Stall and Wake Theory: This combines dynamic stall theory, Eqs. (2) - (4) and dynamic wake theory, Eqs. (8) - (10).

A final comment concerns the computation of equilibrium state inflow. In linear, quasisteady stall, and dynamic stall theories it is computed from the momentum theory, while in the dynamic wake, and dynamic stall and wake theories it is computed, respectively, from the coupled blade-wake and blade-wake-stall equations.

Analysis

For the rigid flap-lag model of the root-flexure-blade assembly, we follow Ref. 2 for the equations of motion including the hinge-offset effects. For the other three models, the equations of flap bending, lag bending and torsion are based on Hamilton's principle with a second-order ordering scheme. The spatial dependence is treated by a Galerkin scheme using the uncoupled nonrotating mode shapes. Development of closed-form expressions of mode shapes is a routine exercise for the spring model. However, for the modified model, we use the closed-form expressions developed in Ref. 3 using

computer algebra; the mode shapes refer to a stepped beam with one end fixed and the other free. At the junction of the blade and the root flexure, there is discontinuity in the distributions of mass and flap-lag-torsion stiffnesses. The closed-form expressions account for this discontinuity and provide continuous displacements, slopes, moments and shear forces. For the modal model, the nonrotating modes are calculated by Myklestad-type and finite element schemes with identical mass and stiffness distributions of the experimental model. The modes from these two schemes agree. Throughout, the Galerkin-type integrals are calculated numerically.

As in the experimental rotor, the analytical model has three blades of the NACA 23012 airfoil section. To include dynamic stall lift, drag and pitching moment, the blade is discretized into five equal-length elements; each element has seven dynamic stall states (three in lift and two each in drag and pitching moment). Using the rigid flap-lag model and the dynamic stall and wake theory, we investigated the convergence characteristics of the lag regressive-mode damping with respect to the number of radial shape functions and spatial harmonics in the wake representation. The wake model with seven harmonics and three shape functions for each harmonic gave results with a maximum error not exceeding 12%. Therefore, the present analysis is based on the dynamic wake representation that has seven harmonics with three radial shape functions for each harmonic; this leads to 45 wake states. Thus, with two modes each in flap bending, lag bending and torsion, the three-blade rotor has 186 states. The airfoil-section quasisteady stall and dynamic stall characteristics of lift, drag and pitching moment for a complete sweep of angle of attack ($-180^0 \le \alpha \le 180^0$) are as in Ref. 3.

The experimental rotor is operated untrimmed with no cyclic pitch control; the collective pitch angle and shaft angle are known control parameters. The periodic response and the Floquet transition matrix for perturbations about that response are generated by periodic shooting. The damping levels are evaluated from the eigenanalysis of the Floquet transition matrix. All the structural and aerodynamic states are included in periodic shooting as well as in eigenanalysis.

Correlation

Reference 6 provides a voluminous database of lag regressive-mode damping of a soft-inplane rotor and includes well over 2000 data points; the test focuses on the forward-flight aspects of the stability problem. To cover the gist of the database, it becomes necessary to include samples of typical cases tested. Accordingly, we include the following cases: collective pitch angle ($0^0 \leq \theta_0 \leq 6^0$), shaft angle ($0^0 \leq \alpha_s \leq 20^0$) and advance ratio ($0 \leq \mu \leq 0.55$). The rotor speed Ω = 1000 rpm, corresponding to a dimensionless lead-lag frequency of 0.61. The structural coupling parameter $\mathcal{R}$= 0; this refers to the database for which the collective pitch angle is set manually by changes to the angle of the blade relative to the root flexure. Low-thrust conditions occur when both collective pitch angle and advance ratio are low or when a combination of high collective pitch angle offsets a high shaft angle. Similarly, high (negative) thrust conditions occur at low collective pitch angle when both advance ratio and shaft angle are high. Thus, the correlation covers near-zero- to high-thrust conditions for various combinations of shaft angle, collective pitch angle and advance ratio.

Rigid Flap-Lag Model

Correlations in Figs. 4-6 are based on the rigid flap-lag model for $\theta_0 = 0^0$, 3^0 and 6^0, respectively. As seen from Fig. 4a for $\alpha_s = 8^0$, the data are available from hover to advance ratio as high as 0.55. The thrust level C_T/σ_s (based on the linear theory) is nearly zero in hover and increases with increasing advance ratio; for example, at μ = 0.55, C_T/σ_s = -0.07. As seen from the data, damping remains nearly constant from hover to $\mu \approx 0.3$ and then increases consistently for $0.3 \leq \mu \leq 0.55$; in fact, it increases sharply for $\mu > 0.4$. For $\mu \leq 0.3$, all the five aerodynamic theories identified in the figure predict nearly the same damping and the correlation is satisfactory. Given the low-thrust conditions ($C_T/\sigma_s \leq -0.03$), this is expected. For $\mu > 0.3$, the differences between these theories begin to manifest and for $\mu > 0.4$ become more marked. The dynamic wake theory, and to some extent the linear theory, initially pick up the trend of the data of increasing damping for $0.3 \leq \mu \leq 0.4$. However, this is followed by a trend of leveling off for $\mu \approx 0.5$ and then of decreasing sharply for $\mu > 0.55$. For $0.3 \leq \mu \leq 0.4$, the remaining three theories are marginally better. But the damping from the quasisteady stall theory decreases for $\mu >$

0.45 and then increases for $\mu \geq 0.55$. The dynamic stall theory initially, say at $\mu \approx 0.5$, shows a slight decrease in damping; then it shows that for $\mu > 0.5$ the damping sharply increases with increasing advance ratio. But the increase is delayed in that it begins to occur at a higher value of μ than indicated by the data. The dynamic stall and wake theory roughly follows the dynamic stall theory despite a hump at $\mu \approx 0.5$ that brings the theory closer to the data and a trough that takes the theory farther from the data.

We continue the correlation in Fig. 4b for $\alpha_s = 16^0$. The data show the trend of constant damping from hover to an advance ratio of 0.25 and of rapidly increasing damping thereafter ($0.25 \leq \mu \leq 0.4$). From hover to an advance ratio of 0.1, owing to very low thrust conditions, all the five theories are virtually identical. With increasing advance ratio or thrust level, the differences among the theories also increase. In fact for $\mu \geq 0.3$, some of these theories differ qualitatively. This is expected; for the present combination of low collective pitch angle and high shaft angle ($\theta_0 = 0^0$ and $\alpha_s = 16^0$), as the advance ratio increases, (negative) thrust level increases and thereby dynamic stall dominates. According to the linear theory, the damping slowly increases for $0.1 \leq \mu \leq 0.35$, and thereafter it sharply deviates from the data: leveling off around $\mu \approx 0.4$ and sharply decreasing for $\mu > 0.425$. The dynamic wake theory is a significant improvement over the linear theory and provides reasonable correlation for the entire data range ($0 \leq \mu \leq 0.4$). It is qualitatively similar to the linear theory in that the increase in damping is followed by a sharp decrease for $\mu \geq 0.45$. Since the data are limited to $\mu \leq 0.4$, it is not possible to evaluate this sharp decrease for $\mu \geq 0.45$. The damping from the quasisteady stall theory sharply decreases for $0.3 \leq \mu \leq 0.4$ and increases for $\mu \geq 0.425$; the increase is so delayed that it makes the quasisteady stall theory unacceptable. Inclusion of dynamic stall dramatically improves the correlation. The dynamic stall, and dynamic stall and wake theories predict the trend of the data, notwithstanding the dips in damping, which occur around $\mu = 0.35$ for dynamic stall theory and around $\mu = 0.4$ for the dynamic stall and wake theory. Overall, excluding the quasisteady stall theory, the predictions in Fig. 4b fall into two groups. In the first group we have the linear and dynamic wake theories, which basically show that damping increases and that this increase is followed by a sharp decrease. In the second group we have the dynamic stall, and dynamic stall and wake theories, which show that damping essentially

increases with increasing advance ratio, although this increase is accompanied by a small dip in damping and is thereby somewhat delayed.

Figure 5 shows the correlation for $\theta_0 = 3^0$. In Fig. 5a, $\alpha_s = 8^0$ and in Fig. 5b, $\alpha_s = 16^0$, and the data are available for $0 \leq \mu \leq 0.25$ and for $0 \leq \mu \leq 0.35$, respectively. In Fig. 5a, the thrust level is relatively low throughout ($C_T/\sigma_s < 0.04$). It is about 0.03 in hover, increases to 0.04 at $\mu = 0.1$ and thereafter continuously decreases with increasing advance ratio, down to nearly zero at $\mu \approx 0.55$. This is well-reflected by satisfactory correlation, which shows that all five theories are more or less identical and that the minor differences among them essentially decrease with increasing advance ratio.

As seen from the data in Fig. 5b, the damping decreases with increasing advance ratio. Because of low collective pitch and high shaft angles, the thrust level, which is about 0.03 in hover, changes to -0.05 at $\mu = 0.35$. The linear and dynamic wake theories are qualitatively inaccurate because within the data range ($0 \leq \mu \leq 0.35$) they predict that damping consistently increases with increasing advance ratio, a trend opposite to that of the data. These two theories do predict the trend of decreasing damping with increasing advance ratio for $\mu > 0.5$; however, this decrease occurs far beyond the data range to be adequate. The other three theories come close to predicting the trend of the data, though the decrease in damping is delayed ($\mu \approx 0.4$). Compared to the linear and dynamic wake theories, the improved performance by the other three theories, in particular by the quasisteady stall theory, is primarily due to including the effects of quasisteady stall drag. The negative thrust level is relatively low ($C_T/\sigma_s \leq -0.05$ at $\mu = 0.35$), and dynamic wake and stall play a relatively minor role. This is, respectively, well-reflected by the closeness between the linear and dynamic wake theories and between the quasisteady stall and dynamic stall theories within the data range. Although, comparatively, the dynamic stall and wake theory gives the best correlation, Fig. 5b also shows that the correlation merits further improvement.

For $\theta_0 = 6^0$, the data are available for $0 \leq \mu \leq 0.15$. Figure 6 shows one typical case at a very high shaft angle of 20^0, in which the damping very slowly decreases with increasing advance ratio. The

quasisteady stall, dynamic stall, and dynamic stall and wake theories provide adequate correlations. By comparison the linear and dynamic wake theories show that damping sharply increases with increasing advance ratio and thus provide inadequate correlations. Concerning these two contrasting trends, the predictions in Fig. 6 are similar to those in Fig. 5b. The dramatically improved performance by the quasisteady stall theory over the linear and dynamic wake theories is due to nonlinear substall drag effects. The difference between the quasisteady stall and dynamic stall theories is due to unsteady lift effects, and the difference between the dynamic stall, and dynamic stall and wake theories is due to downwash effects.

Concerning the predictions in Figs. 4b, 5b and 6 at very high advance ratios (approximately $\mu > 0.5$) a comment is in order. The linear theory and dynamic wake theory show the trend of decreasing damping with increasing advance ratio. By comparison, the quasisteady stall, dynamic stall, and dynamic stall and wake theories show the opposite trend of increasing damping. In the absence of the data it is not possible to validate these trends.

Elastic Root-Flexure-Blade Models

For the same set of data presented thus far, we now take up the correlations based on the elastic blade models of the root-flexure-blade assembly. Specifically, we use the spring model in Figs. 7 - 9, modified model in Figs. 10 - 12 and modal model in Figs. 13 - 15. The focus of the presentation is on the differences in predictions from the rigid and elastic blade models and thereby on the sensitivity of predictions to modeling details. Therefore, some of the common features, such as virtually identical predictions and good correlations at low-thrust conditions, are not explicitly discussed.

Figure 7a shows that the linear theory is qualitatively inaccurate because it predicts that the damping sharply decreases with increasing advance ratio; a trend opposite to that of the data. The dynamic wake theory provides a much better correlation by predicting that damping increases right down to $\mu = 0.5$. However, it also predicts that damping decreases for $\mu > 0.5$, as does the linear theory for $\mu >$

0.3. In other words, at very high advance ratios both linear and dynamic wake theories predict the same trend of decreasing damping with increasing advance ratio. The quasisteady stall theory shows that the damping begins to decrease around $\mu = 0.5$ and once again begins to increase for $\mu > 0.55$, although this increase is beyond the data range. That the dynamic stall theory begins to deviate from the quasisteady stall theory at $\mu \approx 0.45$ and that this deviation increases with increasing μ or C_T/σ_s demonstrates dynamic stall effects. Overall, dynamic stall theory provides adequate correlation, and the inclusion of wake effects, as done in the dynamic stall and wake theory, brings in further improvement.

Figure 7b is basically an amplified version of Fig. 7a, particularly concerning the quasisteady stall and dynamic stall effects. It is clearly seen that the linear theory is qualitatively inaccurate. Although the dynamic wake theory predicts the trend of the data within the data range ($0 \leq \mu \leq 0.4$), it also shows that damping rapidly drops off for $\mu > 0.4$. The quasisteady stall theory predicts the trend of the data; however, for $\mu > 0.3$, its quantitative deviation from the dynamic stall theory increases because of increasing dynamic stall effects. The dynamic stall, and dynamic stall and wake theories provide good correlation.

Figure 8a for $\theta_0 = 3^0$ and $\alpha_s = 8^0$ shows that the linear and dynamic wake theories provide good correlation throughout. Also the quasisteady stall and dynamic stall theories overpredict damping; nevertheless, they predict the trend of the data of nearly constant damping for the entire data range ($0 \leq \mu \leq 0.25$). The dynamic stall and wake theory falls between these two sets of theories by significantly reducing the overprediction by the quasisteady and dynamic stall theories. This overprediction is due to nonlinear substall drag effects. We emphasize that owing to low-Reynolds-number condition of the experiment (Refs. 2 and 7), substall drag is an important consideration in the correlation. As seen from Fig. 8b for $\theta_0 = 3^0$ and $\alpha_s = 16^0$, none of the five theories within the data range ($0 \leq \mu \leq 0.35$) predict clearly that the damping decreases with increasing advance ratio.

Figure 9 shows the correlation for $\theta_0 = 6^0$ and $\alpha_s = 20^0$. The linear and dynamic wake theories show that damping increases with increasing advance ratio from hover to $\mu = 0.4$. This is opposite to the trend of the data, which, though limited to very low advance ratios ($0 \leq \mu \leq 0.15$), show that damping slowly decreases with increasing advance ratio. The quasisteady stall and dynamic stall theories predict the trend of the data despite appreciable overpredictions. The dynamic stall and wake theory significantly reduces these overpredictions. As was the case in Fig. 6, in which the same set of data was correlated on the basis of the rigid flap-lag model, the nonlinear substall drag accounts for much of the differences between the linear theory and quasisteady stall theory; this is a consequence of low-Reynolds-number effects of the test conditions (Refs. 2 and 7). Dynamic stall is not an issue here and unsteady lift effects account for the differences between the dynamic stall and quasisteady stall theories. Similarly, the effects of unsteady lift and downwash account for the differences between the linear theory and dynamic wake theory. The predictions in Fig. 9 are qualitatively similar to those in Fig. 6. Overall, dynamic stall and wake theory provides fairly adequate correlation.

Now we show the correlation for $\theta_0 = 0^0$ from the modified model: $\alpha_s = 8^0$ in Fig. 10a and $\alpha_s = 16^0$ in Fig. 10b. Basically, the linear and dynamic wake theories predict that damping increases initially at about $\mu > 0.2$ as do the data. They also predict that this increase is followed by a sharp decrease. It is this sharp decrease that is not well-supported by the data. For example, while this decrease begins to occur at about $\mu \geq 0.5$ and within the data range ($0 \leq \mu \leq 0.55$) in Fig. 10a, it occurs at about $\mu \geq 0.45$ outside the data range ($0 \leq \mu \leq 0.4$) in Fig. 10b. In contrast, we have the other three theories. In particular, dynamic stall, and dynamic stall and wake theories predict that damping basically increases with increasing advance ratio, although the predictions are accompanied by localized humps and troughs. The quasisteady stall theory more or less follows the dynamic stall theory, but it shows considerable loss in damping at about $\mu = 0.55$ in Fig. 10a and $\mu = 0.4$ in Fig. 10b. Although it shows this loss is followed by a rapid increase, the increase begins to occur in a delayed manner at a higher value of μ than what is indicated by the data. Overall the dynamic stall, and dynamic stall and wake theories give good correlation.

Using the same modified model we continue the correlation for the remaining two sets of data: $\alpha_s = 8^0$ and 16^0 both with $\theta_0 = 3^0$ in Fig. 11 and $\alpha_s = 20^0$ with $\theta_0 = 6^0$ in Fig. 12. Basically, the predictions agree with and lie between the corresponding predictions based on the rigid flap-lag model in Figs. 5 and 6, and on the spring model in Figs. 8 and 9. While the linear and wake theories are satisfactory in Fig. 11a, they are not satisfactory in Fig. 12, as was the case earlier based on the rigid flap-lag and spring models. Moreover Figs. 11a and 12 show that the quasisteady stall and dynamic stall theories predict the trend of the data, although the damping levels are overpredicted owing to nonlinear substall drag effects. The dynamic stall and wake theory appreciably reduces this overprediction and provides good correlation throughout. An exception is Fig. 11b for $\theta_0 = 3^0$ and $\alpha_s = 16^0$, in which the data clearly show that damping decreases with increasing advance ratio. The dynamic stall and wake theory is a significant improvement over the other four theories; still it falls short of predicting the trend of the data within the data range. Dynamic stall is not a major factor and the required improvements merit further study.

Figures 13, 14 and 15 are based on the modal model and confirm the corresponding earlier predictions based on the other three models of the root-flexure-blade assembly. We include them here for completeness and future reference.

Comparison of Structural Models

The preceding correlations in Figs. 4-15 are based on four structural models of the root-flexure-blade assembly, and for each model we used five aerodynamic theories. These fairly exhaustive correlations show that the dynamic stall and wake theory is the best of the five theories. Given this background, we present in Figs. 16-18 a comparative assessment of four structural models based on the dynamic stall and wake theory. Figure 16a for $\theta_0 = 0^0$ and $\alpha_s = 8^0$ shows that the predictions from three elastic models are practically identical and provide good correlation throughout. The rigid flap-lag model also provides fairly adequate correlation. The difference between the predictions from three elastic blade models and those from the rigid blade model is due to blade torsion and bending effects (Ref. 3). To set

the stage for Fig. 16b, we mention that with increasing advance ratio and shaft angle, the negative thrust level increases, as do the effects of dynamic stall. This brings in increased system nonlinearity, and accordingly, damping predictions show increasing sensitivity to changes in blade modeling. This sensitivity is more clearly seen in Fig. 16b, which is for $\theta_0 = 0^0$ and $\alpha_s = 16^0$. Figure 16b also shows that all the four blade models adequately predict the trend of the data and that the modified model gives the best of the correlations.

Figure 17a for $\theta_0 = 3^0$ and $\alpha_s = 8^0$ shows that all four blade models give good correlations and that the spring model slightly overpredicts damping. This overprediction, though not appreciable quantitatively, is consistently observed throughout the data range. In Fig. 17b ($\theta_0 = 3^0$ and $\alpha_s = 16^0$) none of the blade models provides good correlation for the entire data range, and the rigid blade model gives at best fairly adequate correlation. Finally, we come to Fig. 18 for $\theta_0 = 6^0$ and $\alpha_s = 20^0$, in which the data are limited to low advance ratios ($0 \leq \mu \leq 0.15$). It is seen that the modified model and the modal model provide good correlations. The predictions from the rigid flap-lag model are also adequate. However, the rigid-blade-predictions show that the damping very slowly increases with increasing advance ratio. On the other hand, the data show that damping slowly decreases with increasing advance ratio. The trend of the data is predicted by the spring model, but it consistently overpredicts damping. This overprediction is due to the overestimation of root-flexure coupling by the spring model, and it increases with increasing blade pitch; for example, compare Fig. 17a and 17b with Fig. 18 at $\mu = 0$.

Conclusions

The preceding correlation is based on a comprehensive database: $0 \leq \mu \leq 0.55$, $0^0 \leq \theta_0 \leq 6^0$, and $0^0 \leq \alpha_s \leq 20^0$. The predictions are based on the rigid flap-lag model of the root-flexure-blade assembly as well as on three elastic blade models: spring model, modified model and modal model. With each model of the root-flexure-blade assembly, five aerodynamic theories are exercised: linear, quasisteady stall, dynamic stall, dynamic wake, and dynamic stall and wake. The correlation shows the

need to include dynamic stall and wake. Based on the dynamic stall and wake theory, the predictions and related correlations lead to the following specific findings:

1. For nearly the entire database, the rigid flap-lag, modified and modal models provide adequate correlation. The predictions from the modified and modal models are nearly the same and run fairly close to the predictions from the rigid flap-lag model. However, with increasing negative thrust levels, as is the case for combinations of high advance ratio and high shaft angle at $\theta_0 = 0^0$, the modified and modal models provide better correlations.
2. For a set of data points at $\theta_0 = 3^0$ and high shaft angles the trend of the data of decreasing damping with increasing advance ratio is not well-predicted; this merits further study.
3. For $\theta_0 = 0^0$ and high shaft angles, as the advance ratio increases, the effects of negatively stalled conditions increase. Under such conditions the predictions show increasing sensitivity to changes in modeling the root-flexure-blade assembly. Consequently the differences in the predictions from the four models increase with increasing negative thrust conditions.
4. The spring model also provides fairly adequate correlation for the entire database. But it overestimates the bending-torsion couplings of the root flexure. This overestimation brings in increasing quantitative degradation to the correlation with increasing blade pitch angle θ_0.
5. The dynamic stall theory is keyed to the airfoil-section characteristics of lift, drag and pitching moment under quasisteady-stall and dynamic-stalled conditions. Improved representation of these characteristics under the low-Reynolds-number conditions of the experiment merits further research; this offers considerable promise in further improving the correlation.

References

1. Manjunath, A. R., Nagabhushanam, J., Gaonkar, G. H., Peters, D. A. and Su, A., "Flap-Lag Damping in Hover and Forward Flight With a Three-Dimensional Wake," *Journal of the American Helicopter Society*, Vol. 38, (4), Oct 1993.

2. Barwey, D., Gaonkar, G. H. and Ormiston, R. A., "Investigation of Dynamic Stall Effects on Isolated Rotor Flap-Lag Stability with Experimental Correlation," *Journal of the American Helicopter Society*, Vol. 36, (4), Oct 1991.

3. Barwey, D. and Gaonkar, G. H., "Effects of Dynamic Stall and Structural Modeling on Helicopter Blade Stability with Experimental Correlation," *AIAA Journal*, Vol. 32, (5), May 1994 (in press), also see proceedings of the American Helicopter Society 48th Annual Forum, Washington, DC, Jun 3-5, 1992.

4. Torok, M. S. and Chopra, I., "Hingeless Rotor Aeroelastic Stability Analysis With Refined Aerodynamic Modeling," *Journal of the American Helicopter Society*, Vol. 36, (4), Oct 1991.

5. Peters, D. A. and Su, A., "The Effect of Hidden Dynamic States of Floquet Eigenvalues," *Journal of the American Helicopter Society*, Vol. 35, (4), Oct 1990.

6. McNulty, M. J., "Flap-Lag Stability Data for a Small Scale Isolated Hingeless Rotor in Forward Flight," NASA TM 102189, Apr 1989.

7. Gaonkar, G. H., McNulty, M. J. and Nagabhushanam, J., "An Experimental and Analytical Investigation of Isolated Rotor Flap-Lag Stability in Forward Flight," *Journal of the American Helicopter Society*, Vol. 35, (2), May 1990.

8. Manjunath, A. R., Nagabhushanam, J., Gaonkar, G. H., Chunduru, Srinivas and Prasad Sampath, "Flap-Lag-Torsion Stability in Hover and Forward Flight With a Three-Dimensional Wake," Proceedings of the American Helicopter Society Aeromechanics Specialists Conference, San Francisco, CA, Jan 18-21, 1994.

9. Tang, D. M. and Dowell, E. H., "Damping Prediction For Stalled Rotor Flap-Lag Stability with Experimental Correlation," Private Communication, Jan 10, 1994.

10. Peters, D. A., "Toward a Unified Lift Model for Use in Rotor Blade Stability Analysis," *Journal of the American Helicopter Society*, Vol. 30, (3), Jul 1985.

11. Petot, D., "Differential Equation Modeling of Dynamic Stall," ONERA, Technical Note No. 5, 1989.

12. Peters, D. A., Boyd, D. D. and He, C. J., "Finite-State Induced-Flow Model for Rotors in Hover and Forward Flight," *Journal of the American Helicopter Society*, Vol. 34, (4), Oct 1989.

13. Barwey, D., *Dynamic Stall Effects on Hingeless Rotor Stability With Experimental Correlation*, Ph.D. Dissertation, College of Engineering, Florida Atlantic University, Boca Raton, FL, Apr 1992.

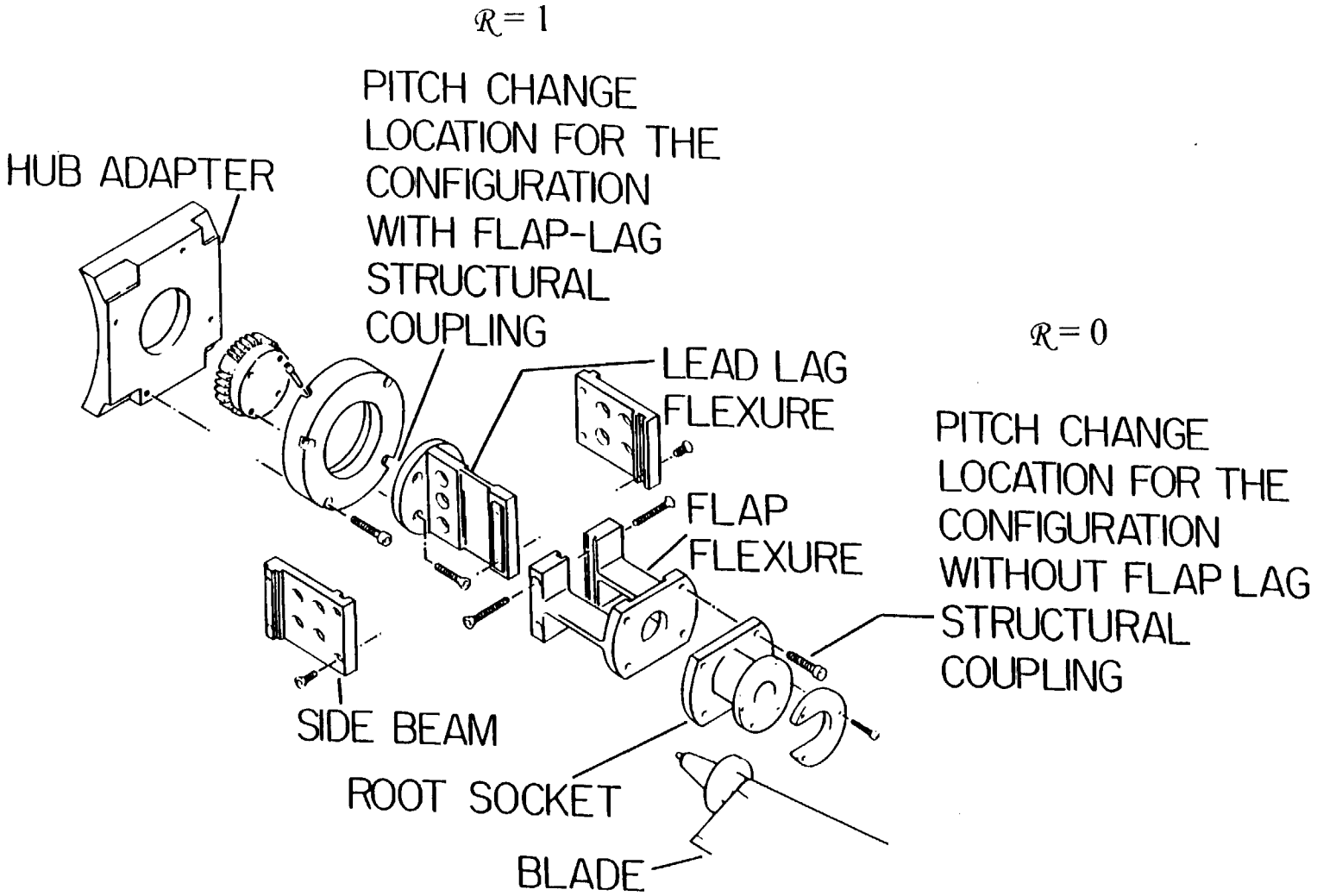

Fig. 1 Exploded View of Root-Flexure-Blade Assembly

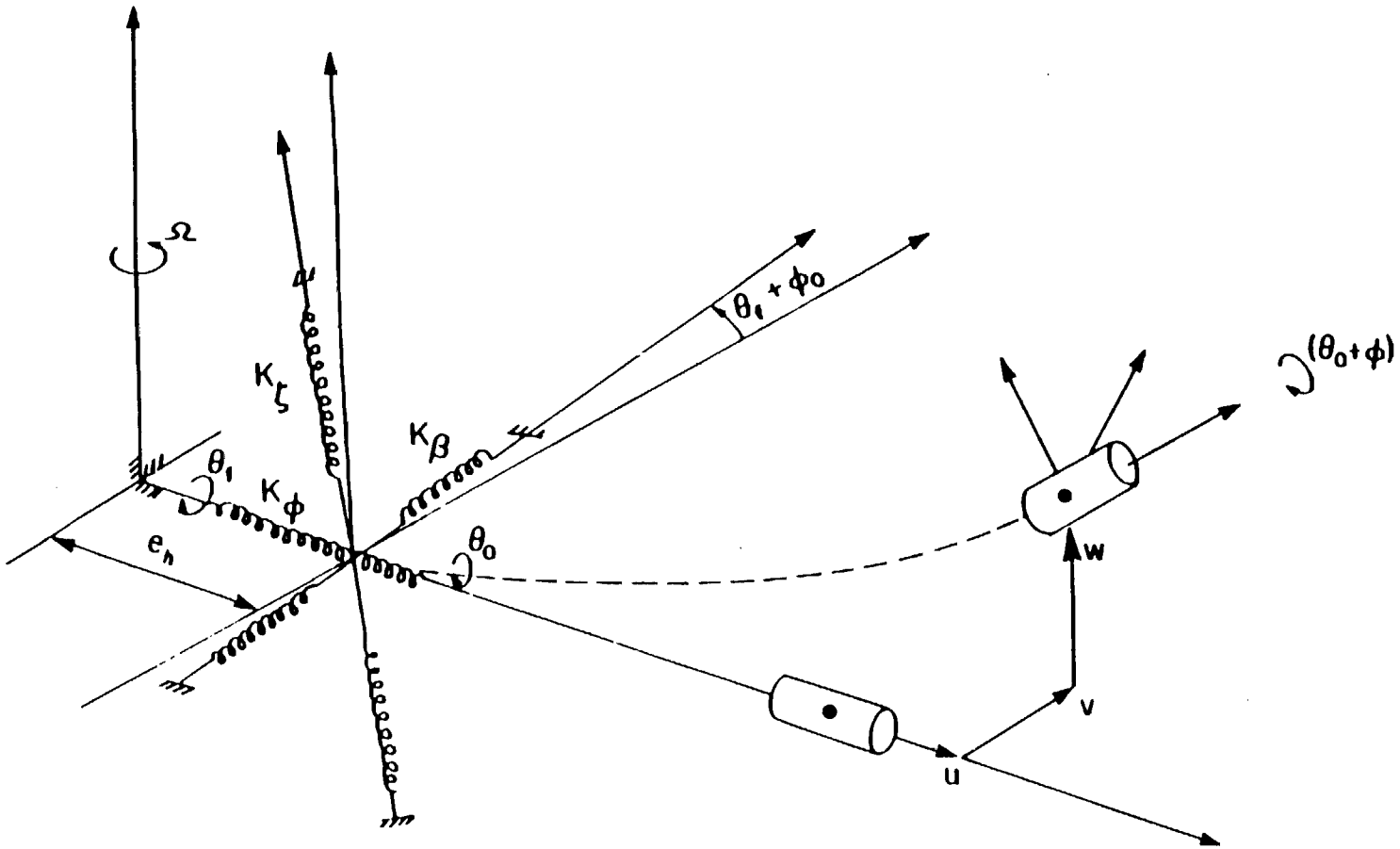

Fig. 2a Schematic of Spring Model

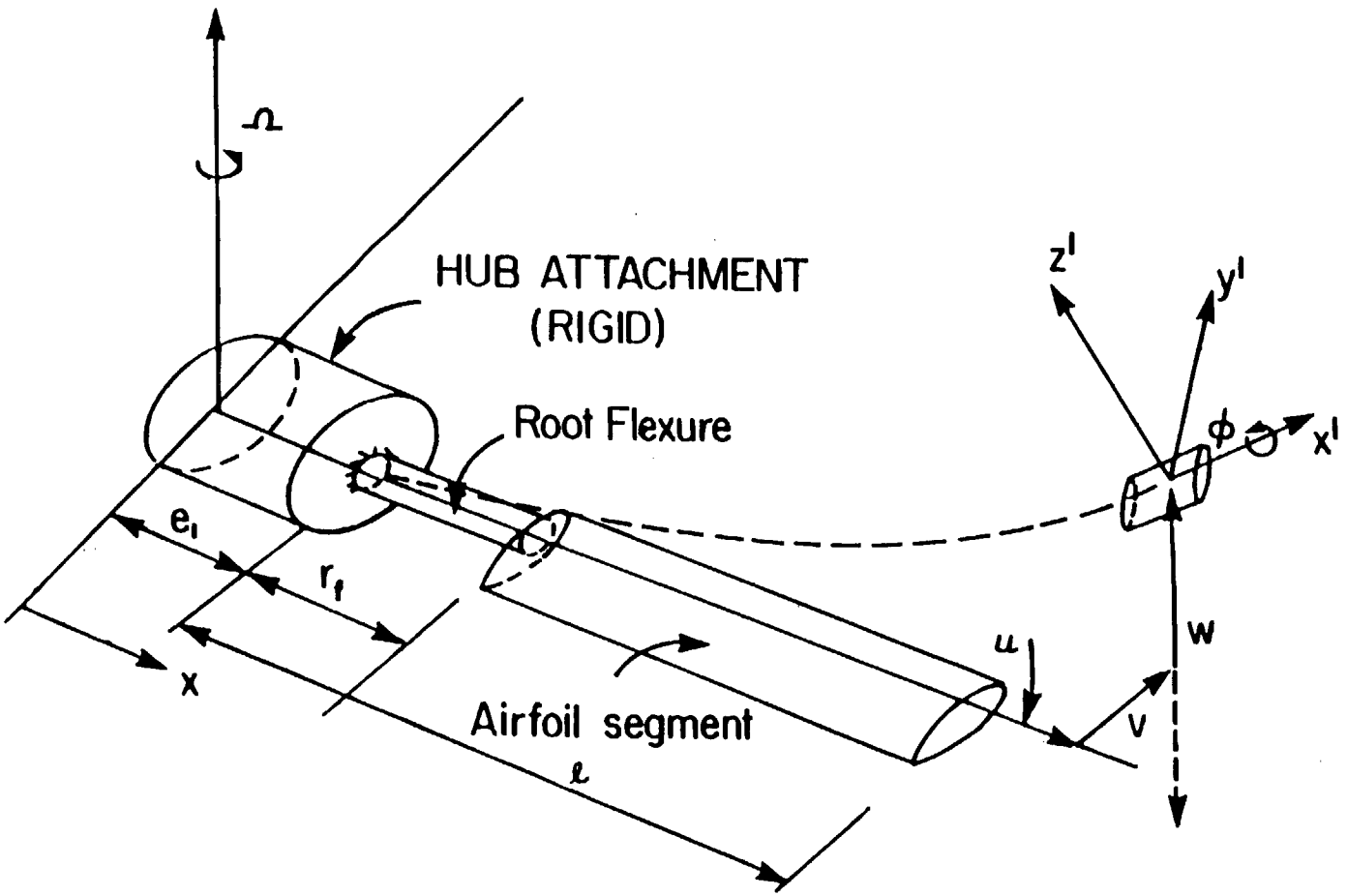

Fig. 2b Schematic of Modified Model

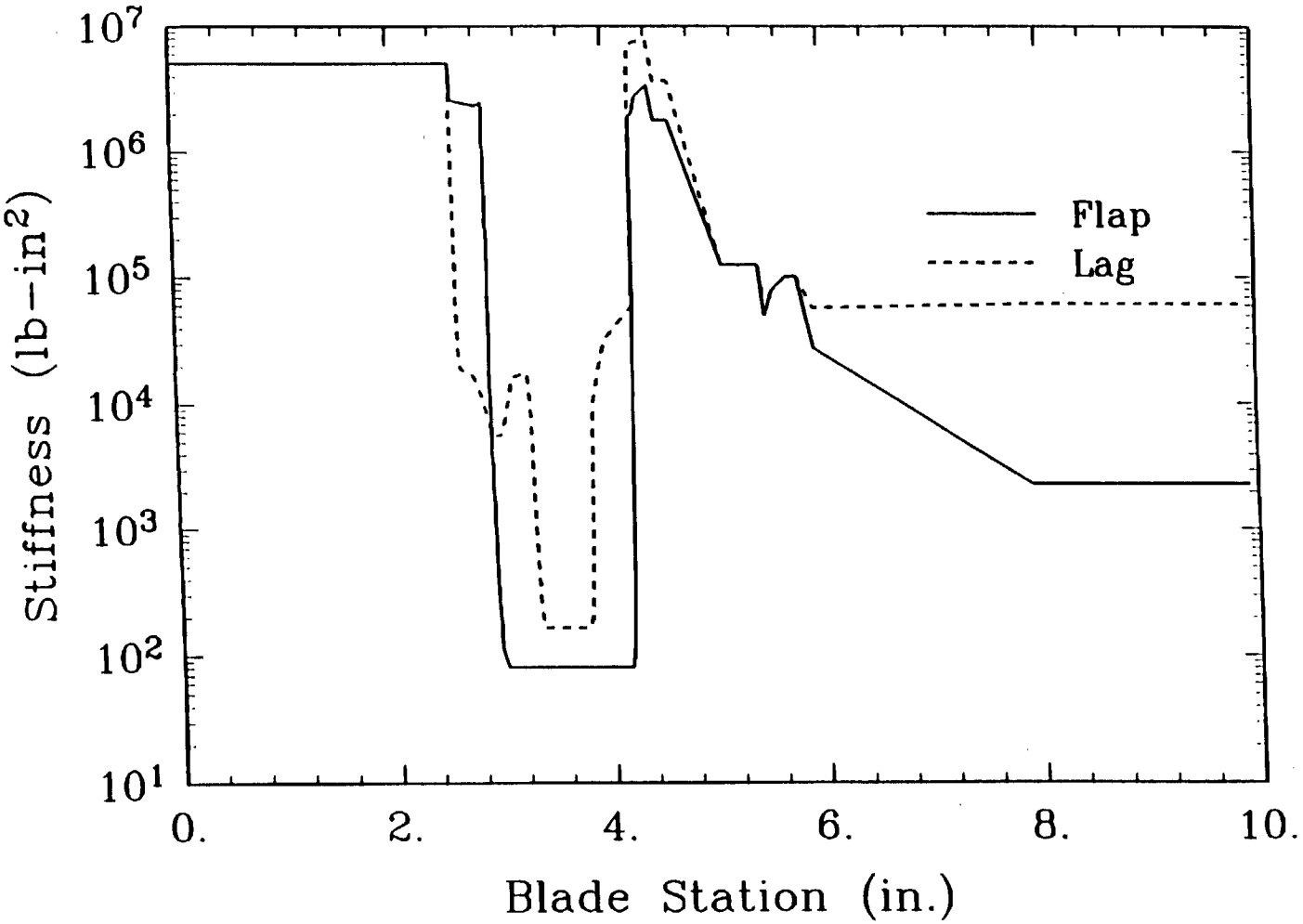

Fig. 2c Stiffness Distributions in the Root Region of the 3-Blade Rotor

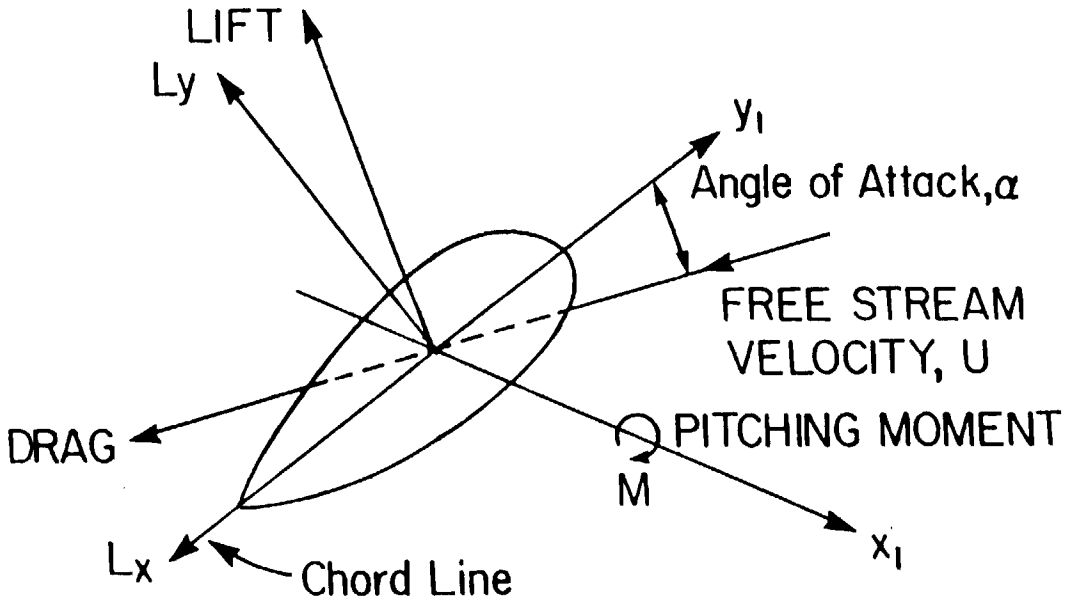

Fig. 3 Schematic of Blade Section Aerodynamics

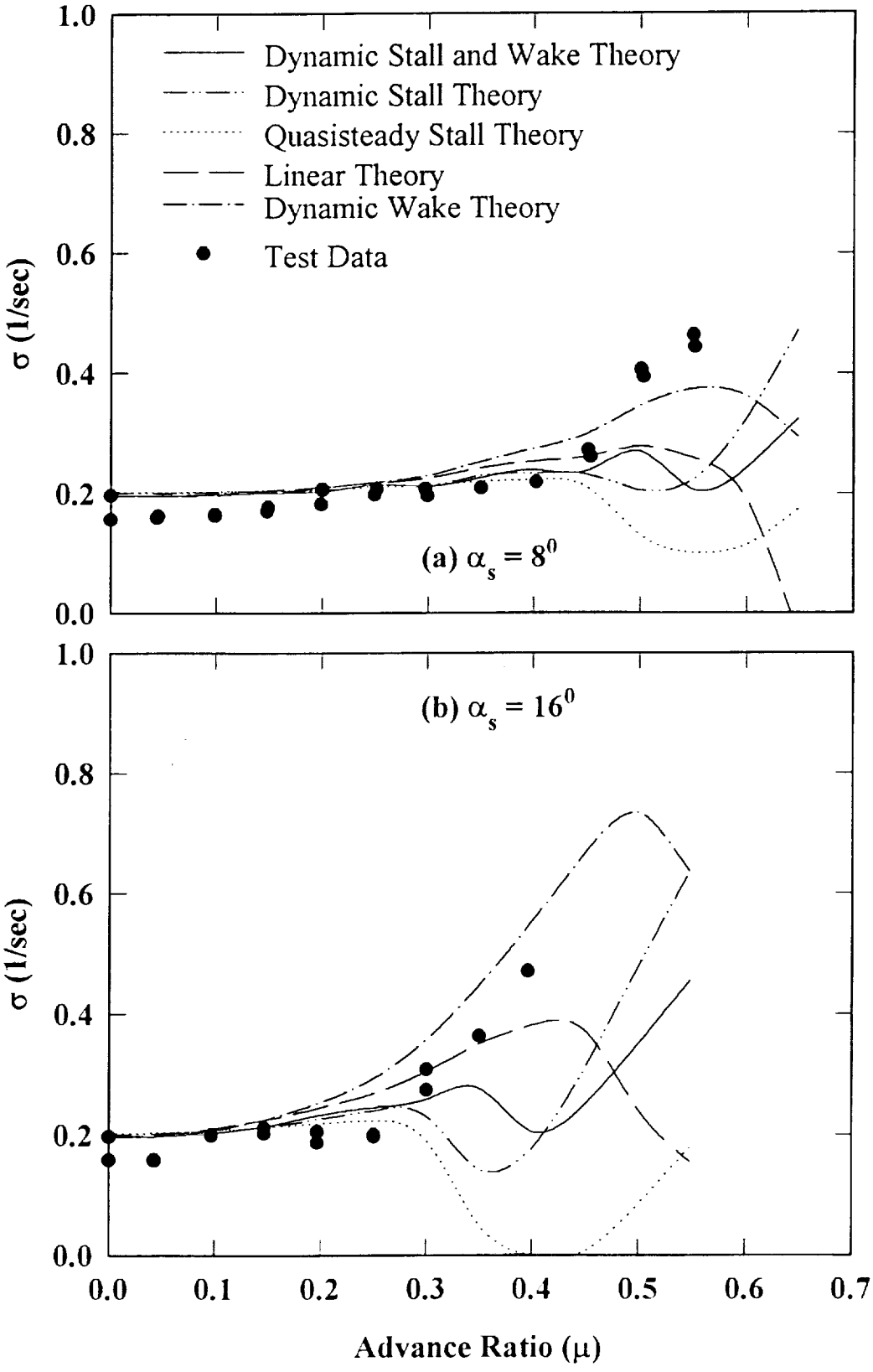

Fig. 4 Effects of Aerodynamic Modeling on Lag Damping Correlation from Rigid Flap-Lag Model with $\theta_0 = 0^0$.

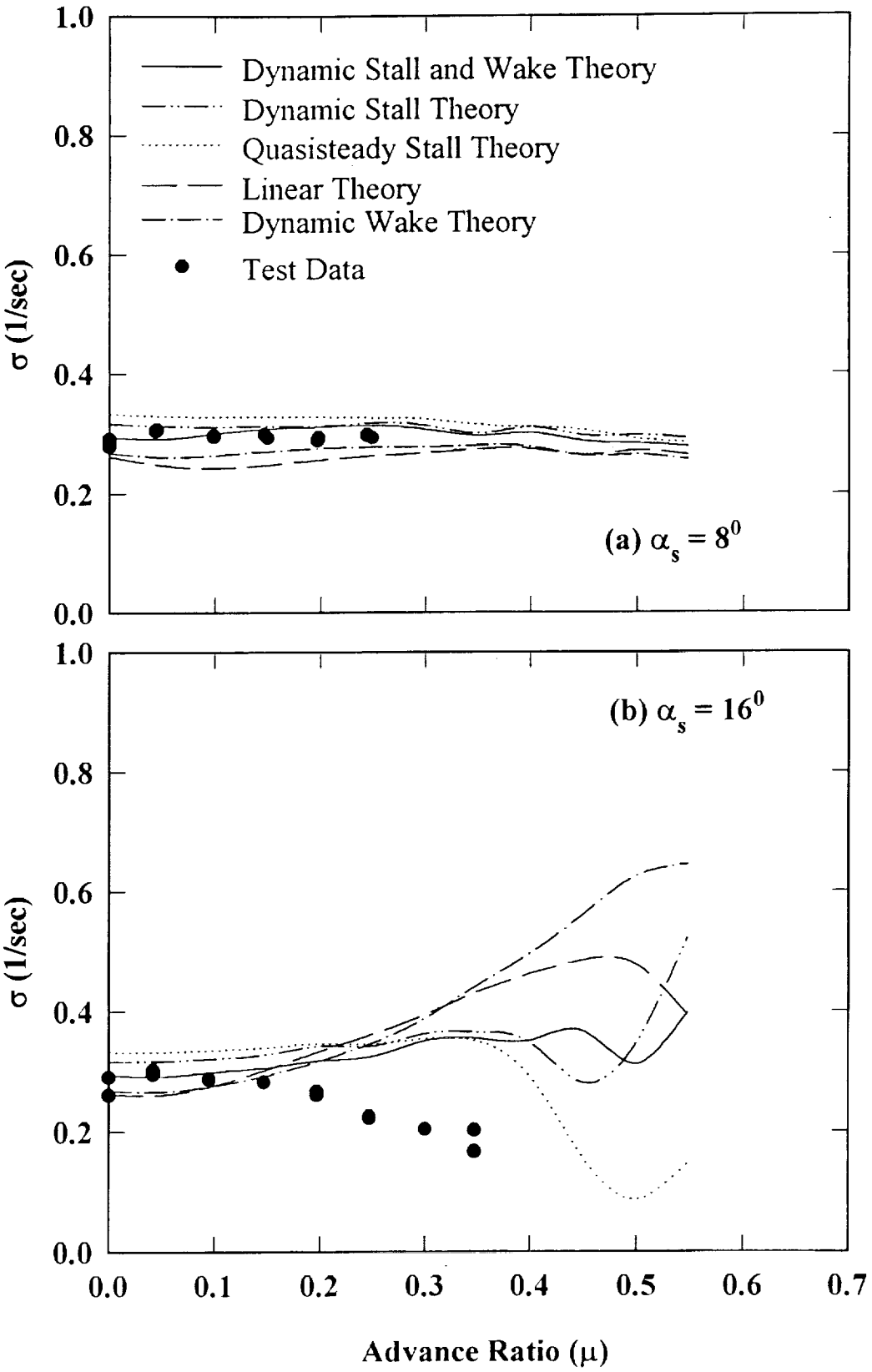

Fig. 5 Effects of Aerodynamic Modeling on Lag Damping Correlation from Rigid Flap-Lag Model with $\theta_0 = 3^0$.

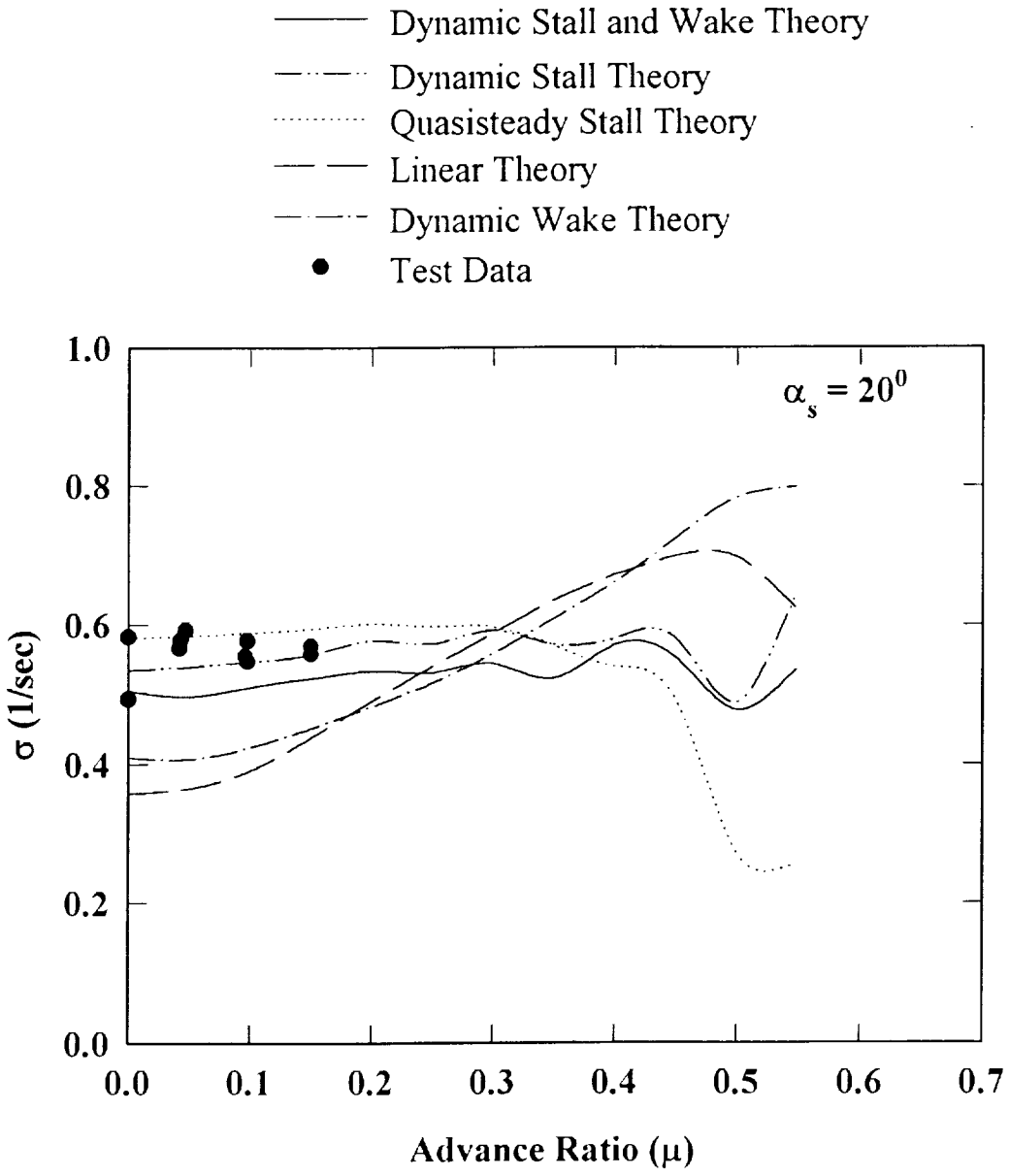

Fig. 6 Effects of Aerodynamic Modeling on Lag Damping Correlation from Rigid Flap-Lag Model with $\theta_0 = 6^0$.

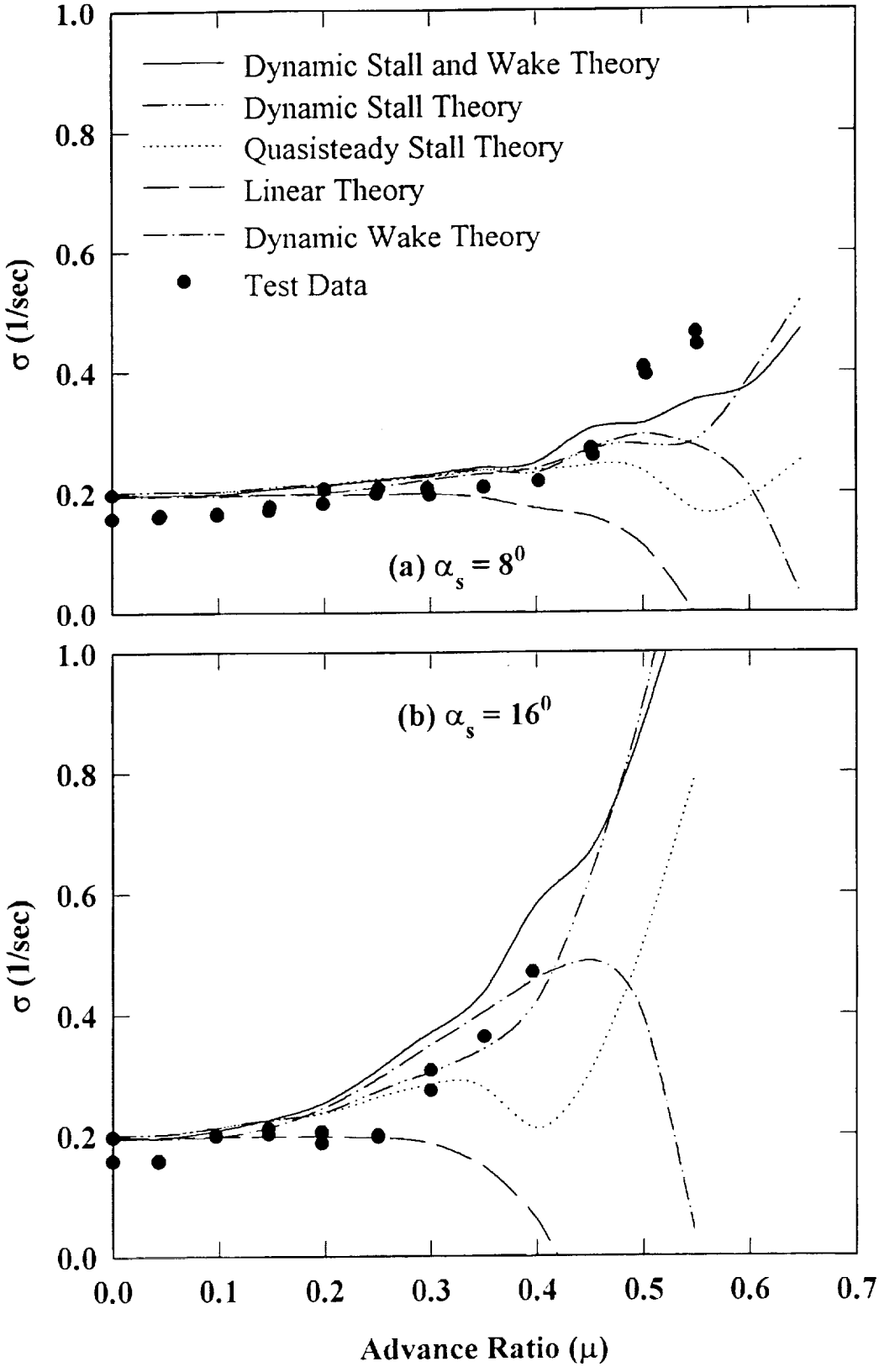

Fig. 7 Effects of Aerodynamic Modeling on Lag Damping Correlation from Spring Model with $\theta_0 = 0^0$.

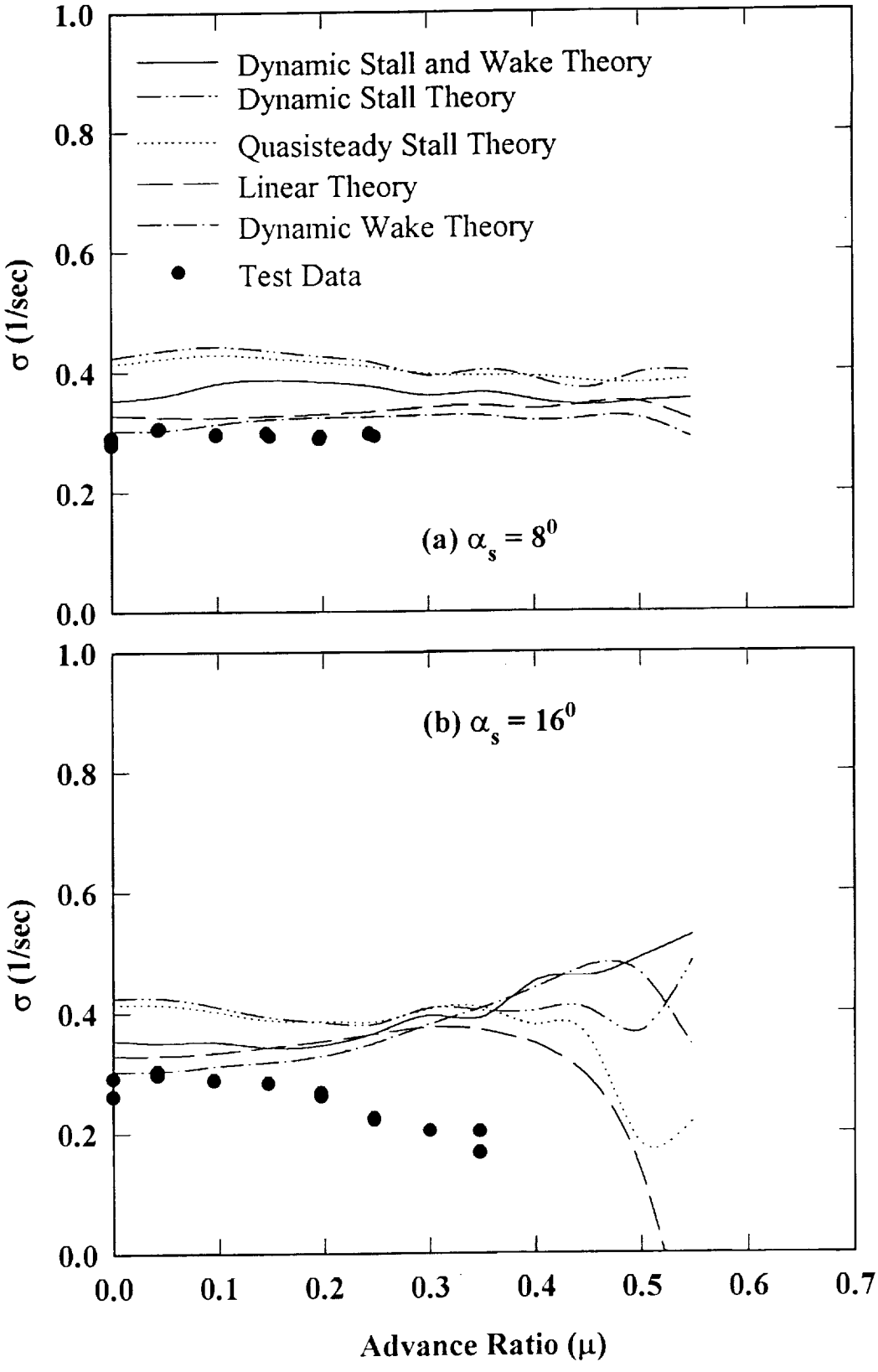

Fig. 8 Effects of Aerodynamic Modeling on Lag Damping Correlation from Spring Model with $\theta_0 = 3^0$.

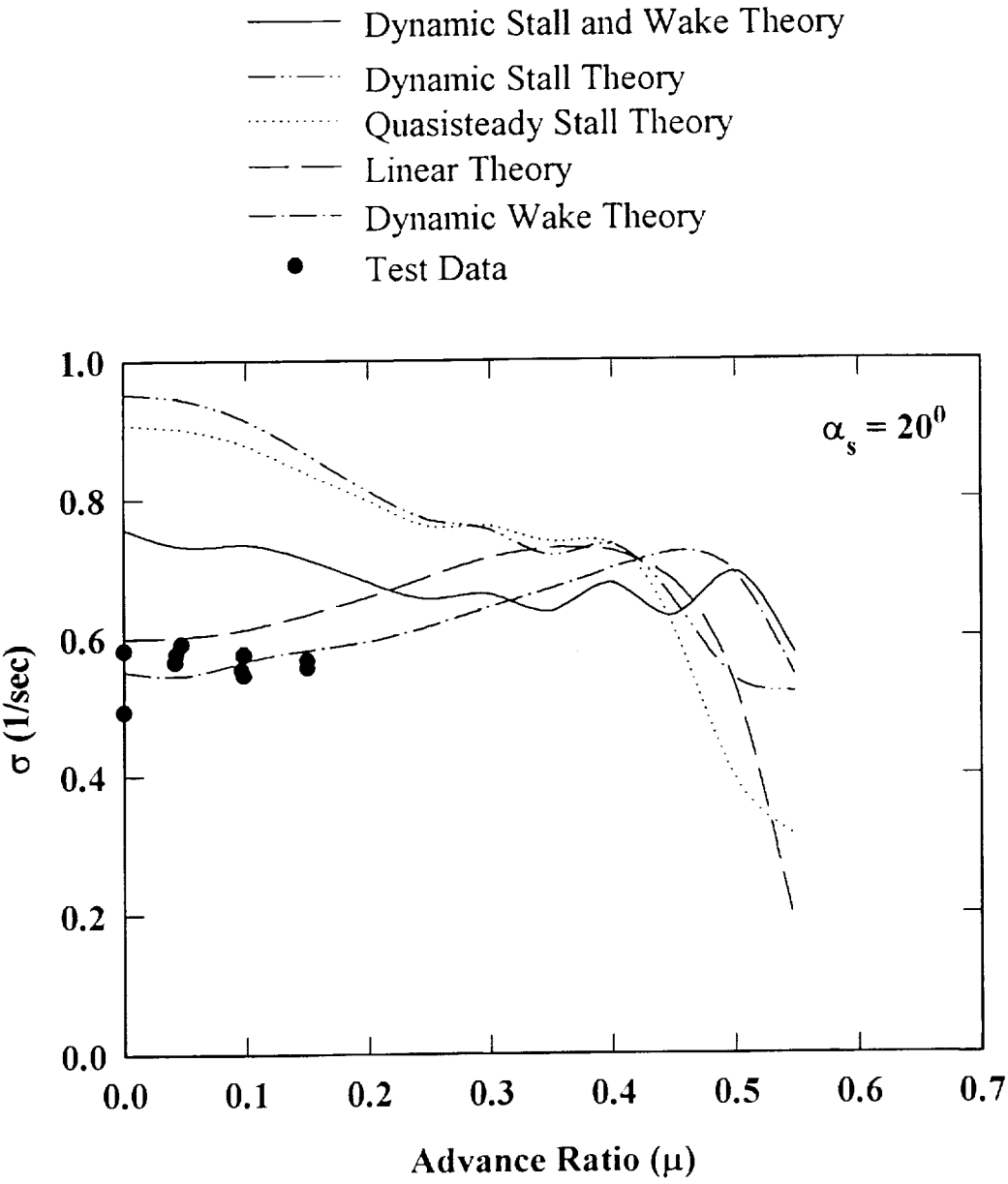

Fig. 9 Effects of Aerodynamic Modeling on Lag Damping Correlation from Spring Model with $\theta_0 = 6^0$.

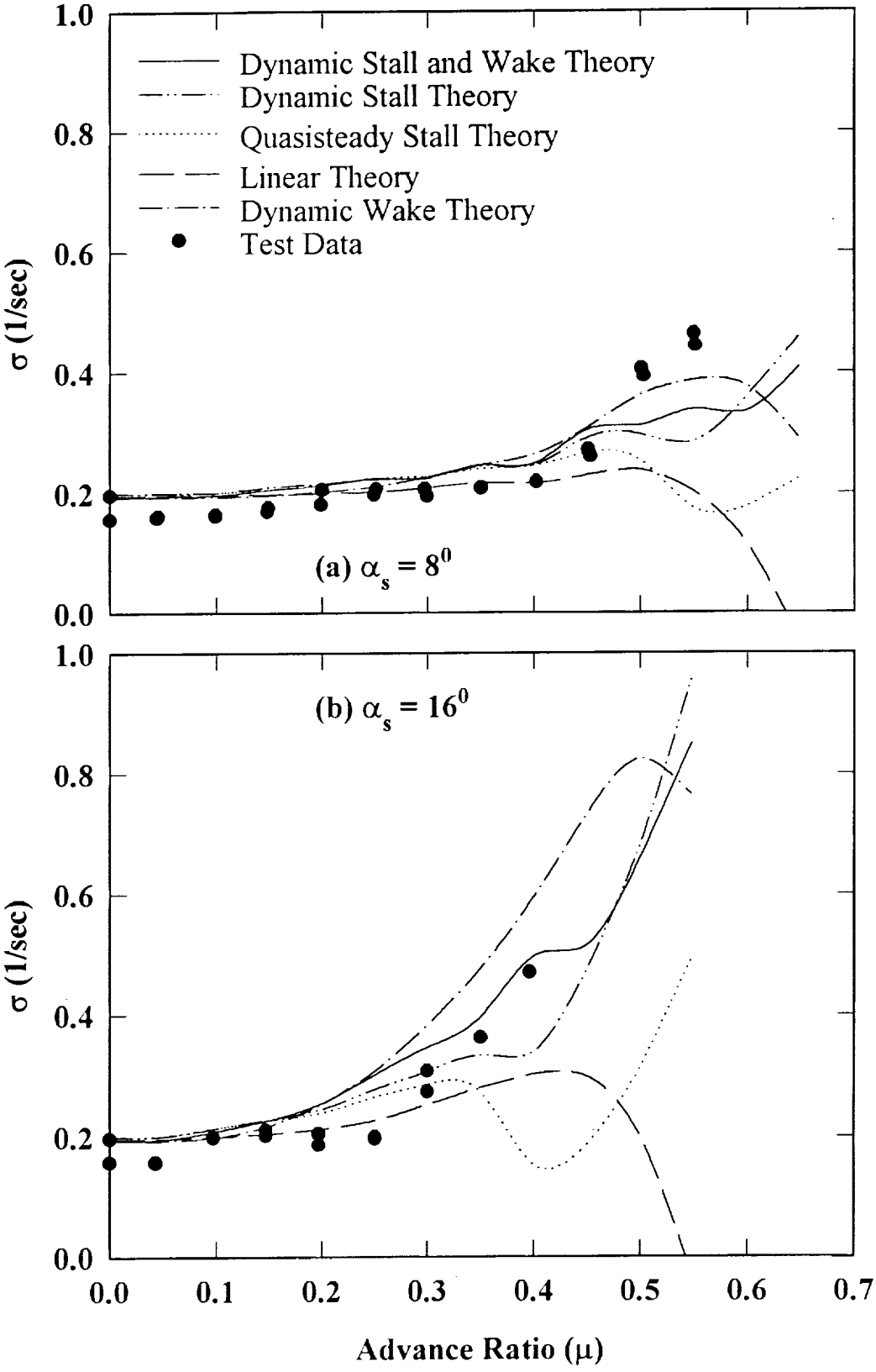

Fig. 10 Effects of Aerodynamic Modeling on Lag Damping Correlation from Modified Model with $\theta_0 = 0^0$.

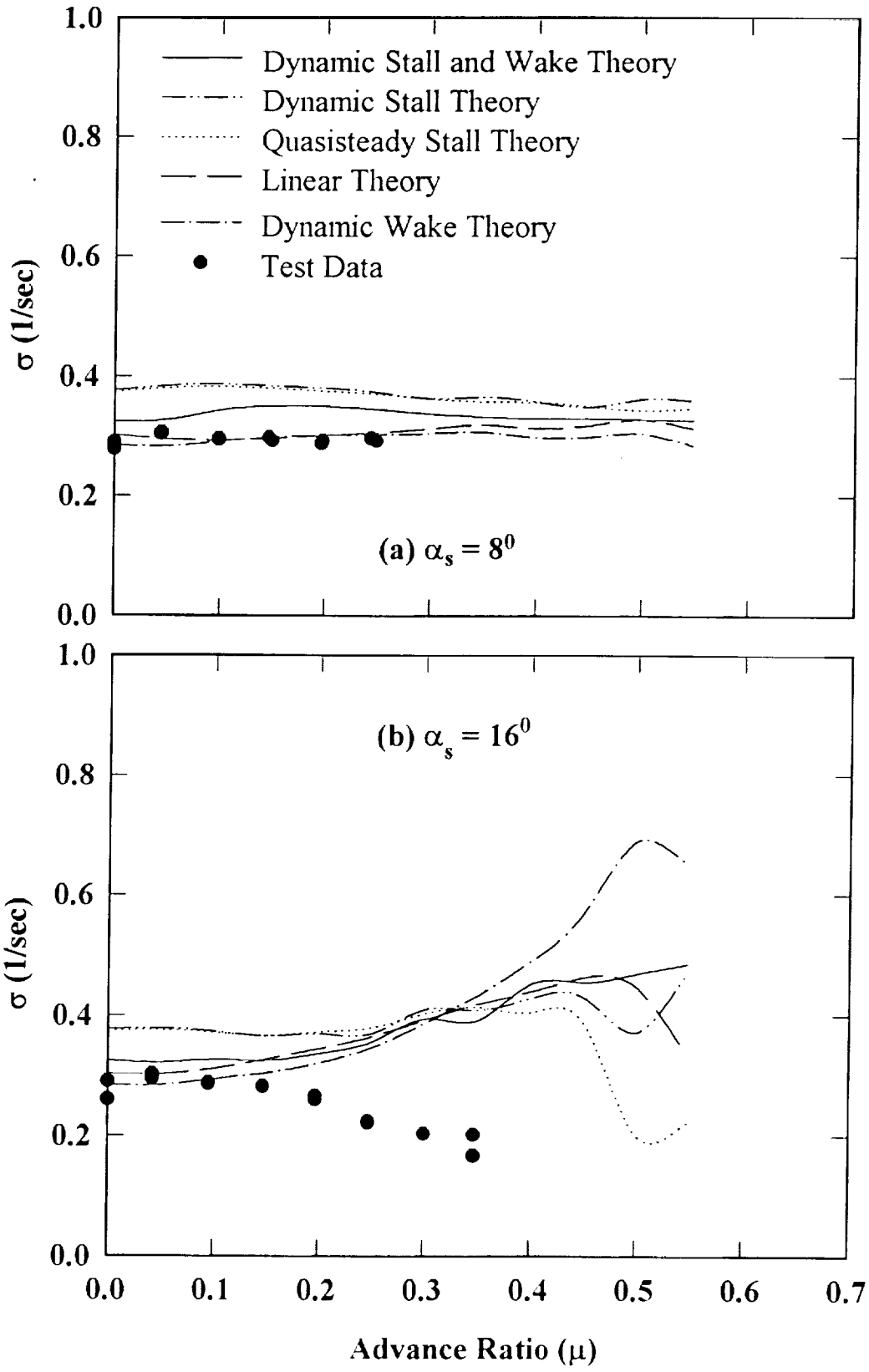

Fig. 11 Effects of Aerodynamic Modeling on Lag Damping Correlation from Modified Model with $\theta_0 = 3^0$.

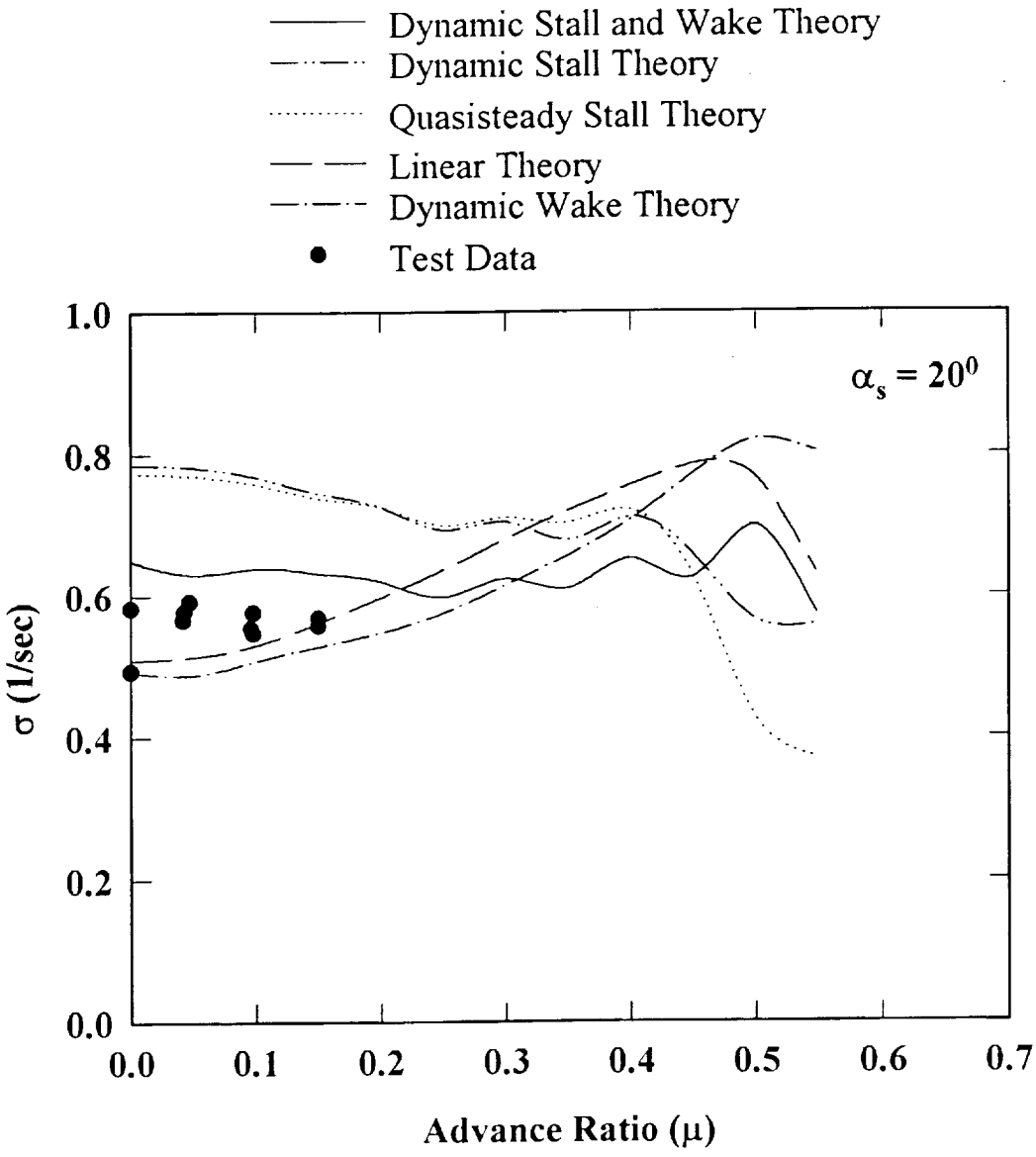

Fig. 12 Effects of Aerodynamic Modeling on Lag Damping Correlation from Modified Model with $\theta_0 = 6^0$.

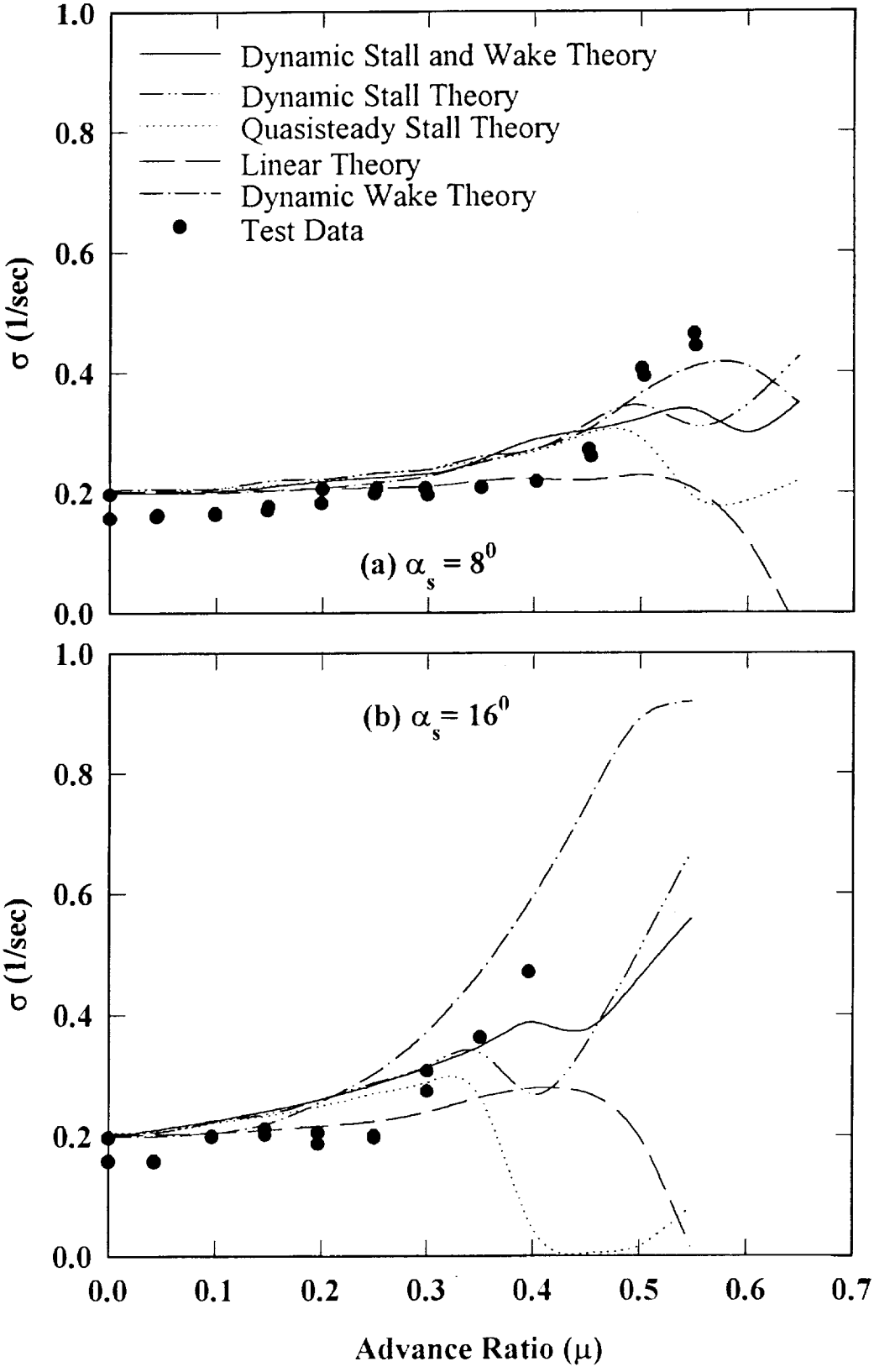

Fig. 13 Effects of Aerodynamic Modeling on Lag Damping Correlation from Modal Model with $\theta_0 = 0^0$.

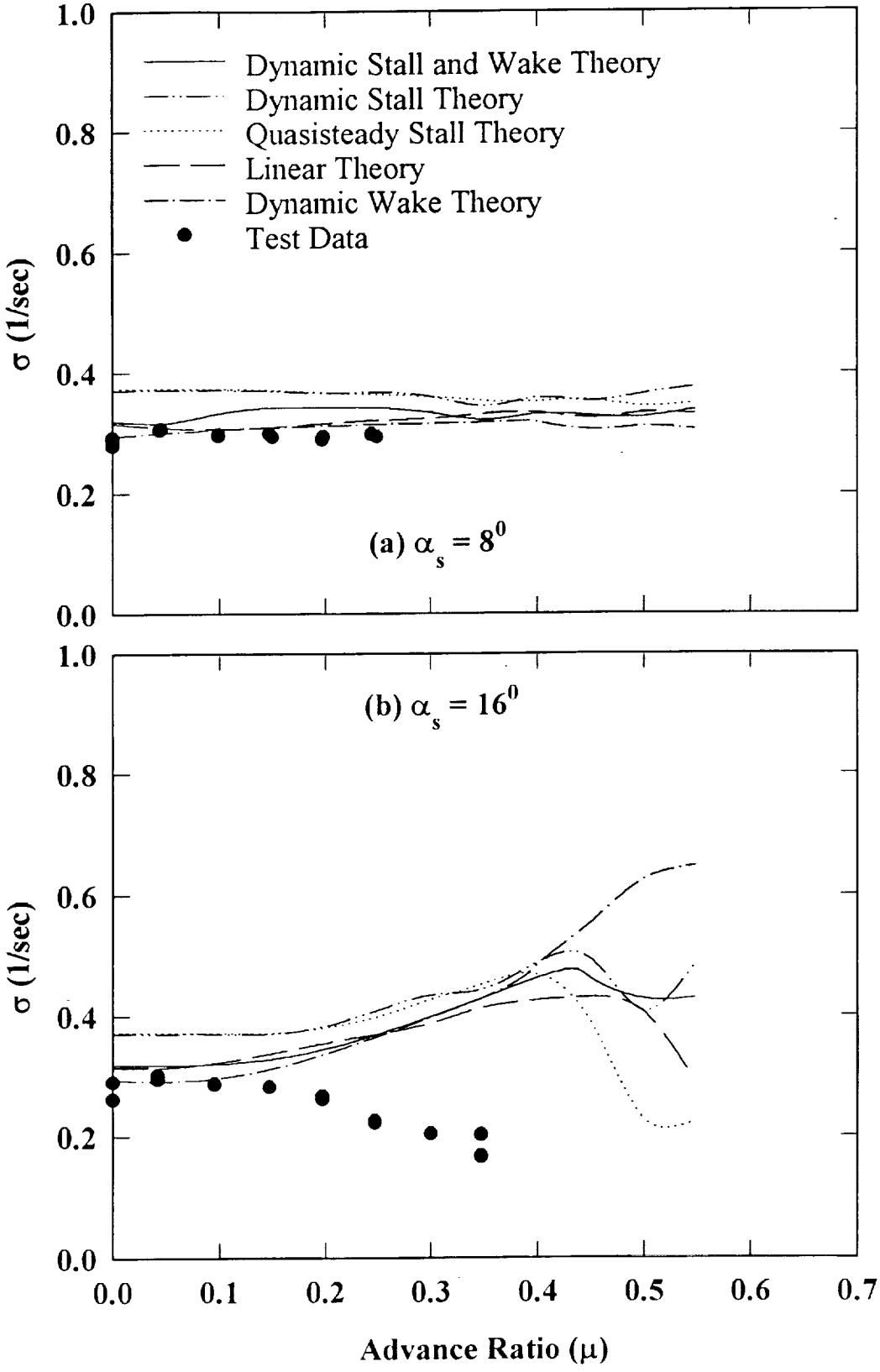

Fig. 14 Effects of Aerodynamic Modeling on Lag Damping Correlation from Modal Model with $\theta_0 = 3^0$.

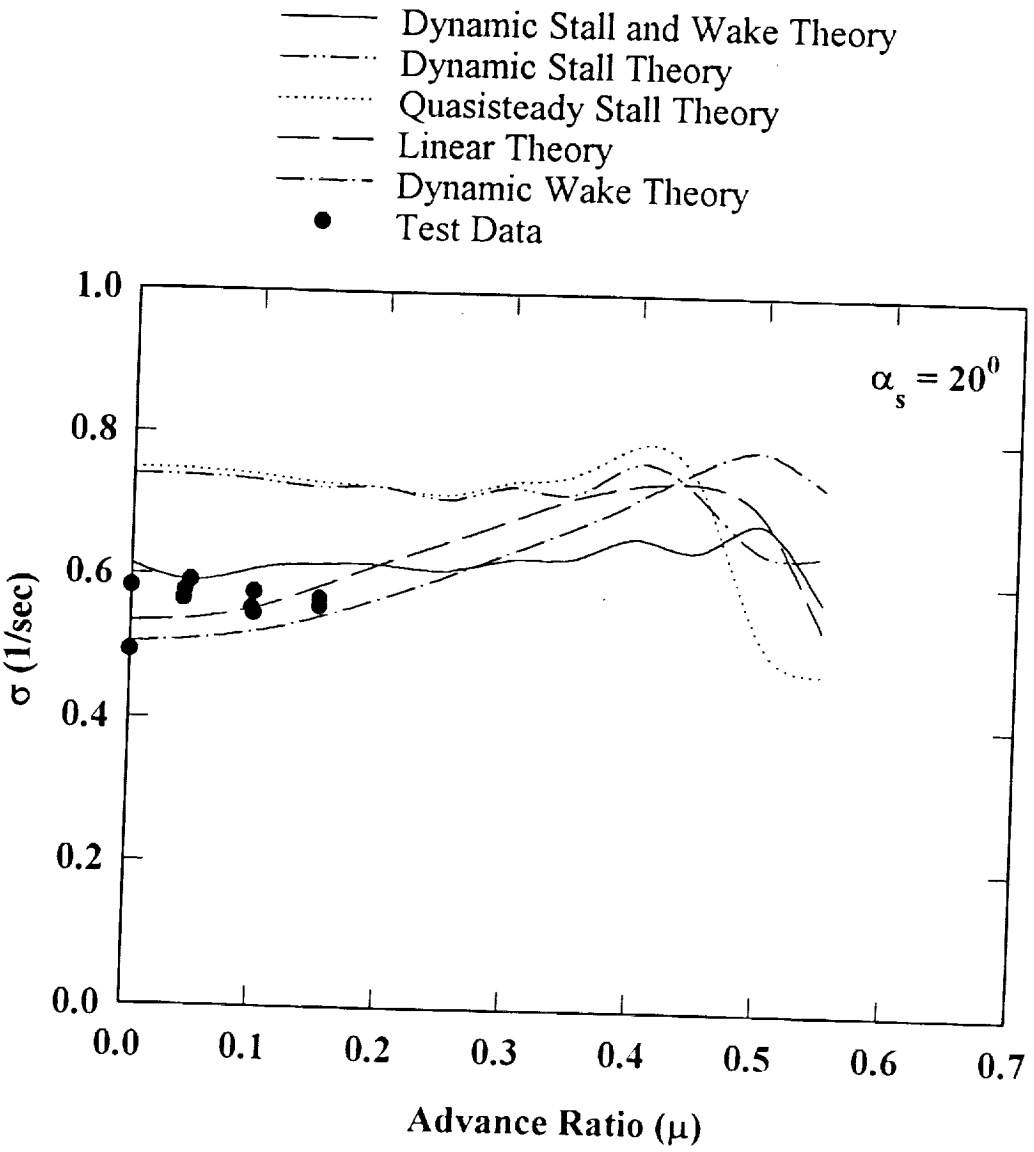

Fig. 15 Effects of Aerodynamic Modeling on Lag Damping Correlation from Modal Model with $\theta_0 = 6^0$.

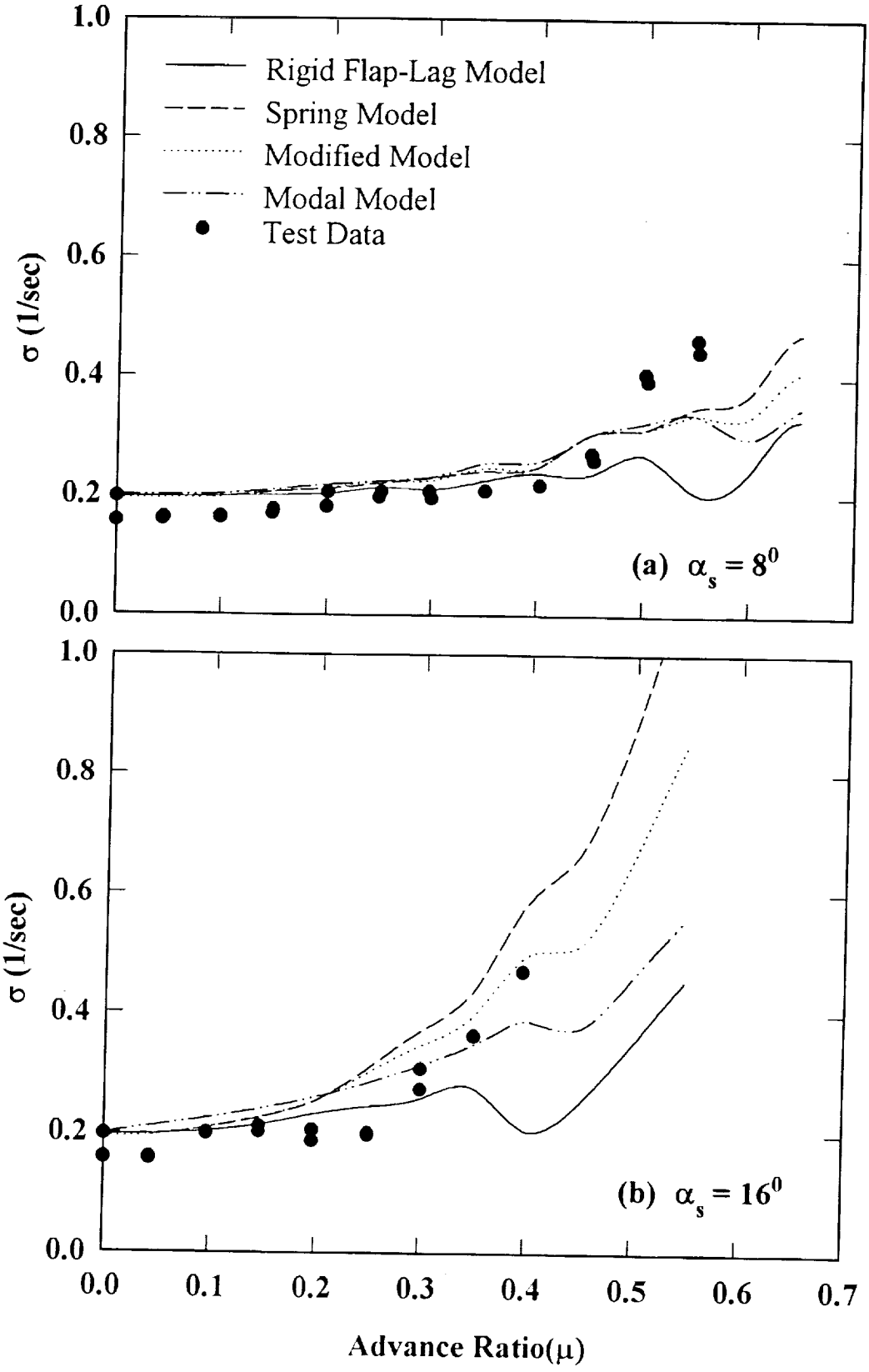

Fig. 16 Effects of Structural Modeling on Lag Damping Correlation from Dynamic Stall and WakeTheory with $\theta_0 = 0^0$.

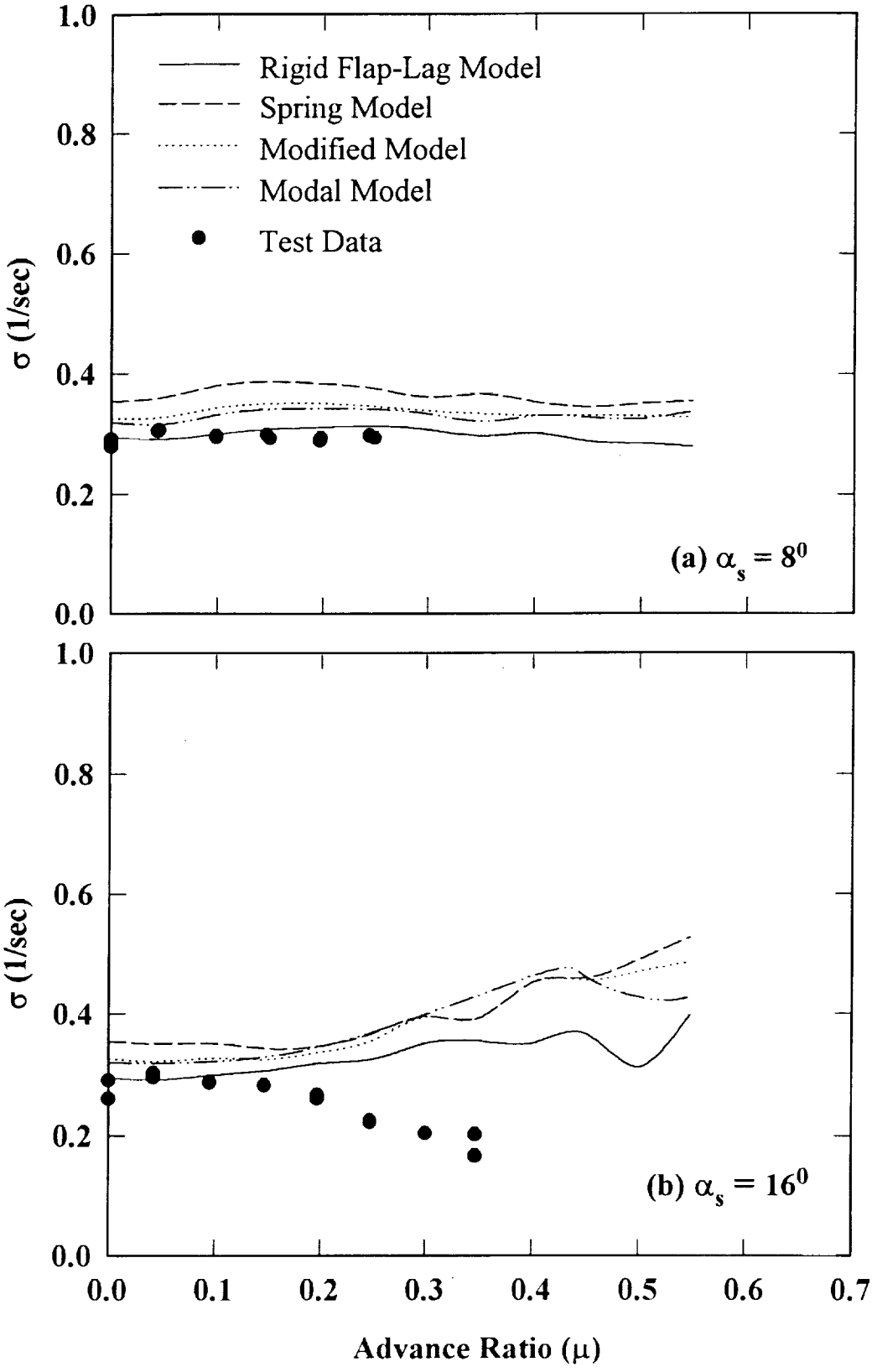

Fig. 17 Effects of Structural Modeling on Lag Damping Correlation from Dynamic Stall and Wake Theory with $\theta_0 = 3^0$.

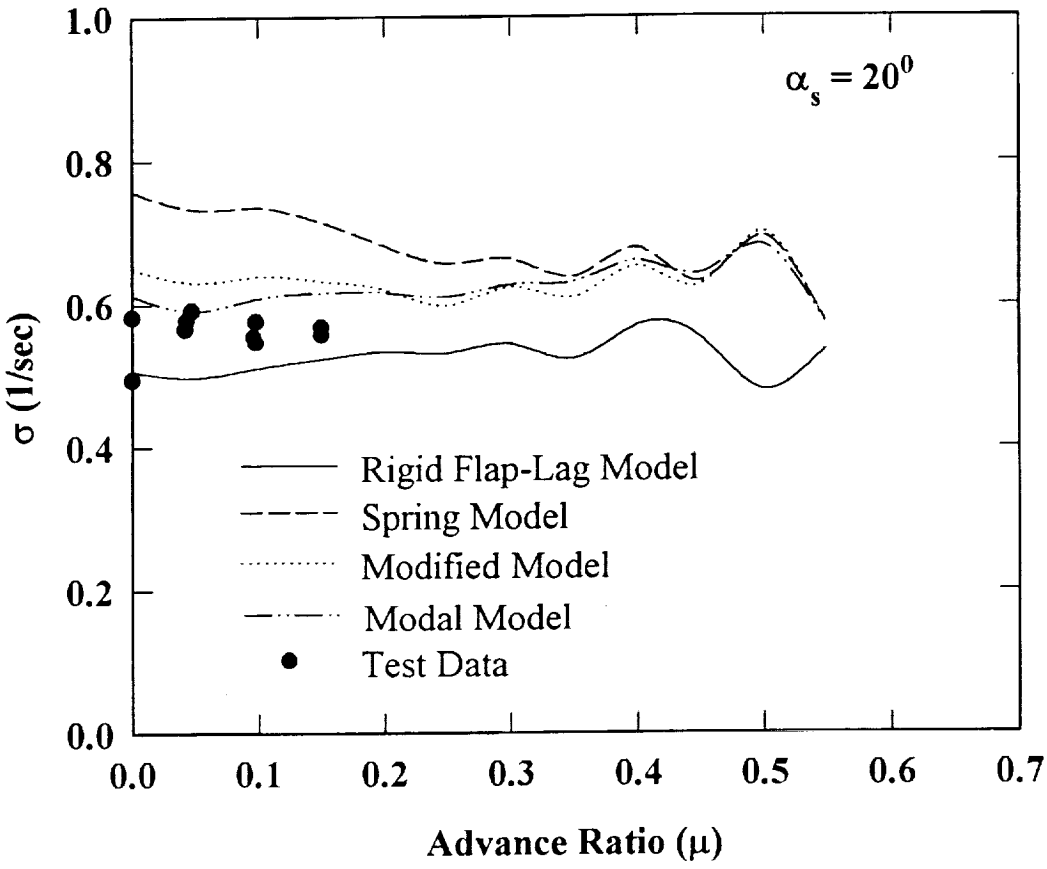

Fig. 18 Effects of Structural Modeling on Lag Damping Correlation from Dynamic Stall and Wake Theory with $\theta_0 = 6^0$.